약학박사학위논문

분비된 AIMP1의 발모 효과 연구

The novel activities of the secreted AIMP1 for hair growth

서울대학교 융합과학기술대학원

분자의학 및 바이오제약학과 세포유전체학전공

김 윤 하

Abstract

Hair follicle stem cells (HFSCs) and dermal papilla cells (DPCs) are crucial for the biogenesis and maintenance of hair follicles (HFs). However, crosstalk between the two cells is not fully understood. Here, we found that a peptide derived from Aminoacyl-tRNA synthetase-Interacting Multi-functional Protein 1 (AIMP1) is secreted from HFSCs to activate DPCs for the maintenance of HFs. *In vivo* analysis revealed that the AIMP1 level was decreased in HFs with age and hair loss. The N-terminal 192-amino acid peptide fragment of AIMP1 is generated by matrix metalloproteinase 2 and secreted from the WNT-activated HFSCs to activate DPCs via fibroblast growth factor receptor 2. Deletion mapping revealed 41 amino acids (TN41, from Ala6 to Lys46) as the active region. This region activated the AKT and extracellular-signal-regulated kinase (ERK) pathway, increasing the level of beta-catenin and inducing the proliferation of DPCs. Taken together, the AIMP1 fragment secreted from HFSCs stimulates the hair cycle into active hair growth phases.

Keywords: ARS-Interacting Multi-functional Protein 1, Hair growth, Hair follicle, Hair follicle stem cell, Dermal papilla cell, Secretion, Fibroblast growth factor receptor 2, ERK, AKT, beta catenin

Student Number: 2011-31339

Contents

Introduction

Hair follicle stem cells (HFSCs), which reside in the bulge/sub-bulge area of the hair follicle (HF), sustain cyclic hair regrowth over repeated hair cycles [1-3]. It has been reported that mouse HFSCs generally do not display apparent decreases in numbers [4], but with aging, hair cycle waves slow down and display imbalanced cytokine signaling in HFSCs, as well as diminished colony-forming capability *in vitro* [5-7]. In contrast, mammals that live longer lose their hair and HFs with age [8, 9].

Aminoacyl-tRNA synthetase-Interacting Multi-functional Protein 1 (AIMP1) was originally identified as a member of the mammalian multi-ARS complex [10]. AIMP1 is secreted in response to hypoxia and cytokine stimulation; it functions as a cytokine with various target cells including endothelial cells, monocyte macrophage cells, dendritic cells, and pancreatic cells [11-18]. Recently, macrophages were shown to secrete AIMP1 following stimulation with tumor necrosis factor-α (TNF-α) in wound lesions to enhance wound healing; this process was mediated by fibroblast proliferation and collagen synthesis via AKT and extracellular signal-regulated kinase (ERK) activation [12]. Deletion mapping analysis showed that the N-terminal domain (amino acids 6–46) of AIMP1 was responsible for stimulating fibroblast and mesenchymal stem cell (MSC) proliferation [19, 20]. MSC stimulation occurs via

fibroblast growth factor receptor 2 (FGFR2)−mediated ERK and AKT activation, which results in the accumulation of beta−catenin [20].

Because the signaling pathway involved in beta−catenin via FGFR2 is critical in the HF niche [21−24], we evaluated whether AIMP1 functions in the HFSC niche. We found that AIMP1 is closely correlated with the health and age of HFs in mice. Truncated AIMP1 peptide was secreted from HFSCs and stimulated beta−catenin signaling pathway via FGFR2−mediated activation of ERK and AKT of DPCs. This mechanism promotes the transition from the telogen to anagen phase to achieve active hair growth.

Material & Method

Animals

C57BL/6 mice were purchased from Orient bio (Sungnam, Korea). TCF/LEF1-GFP mice were purchased from Jackson Laboratories (Bar Harbor, ME, USA). Animal care was conducted in accordance with the guidance of Seoul National University. All animal experiments were performed following the Guidelines for the Care and Use of Laboratory. Offspring were genotyped by PCR-based assays of mouse tail DNA.

Generation of inducible hAIMP1 mouse

For generation of inducible hAIMP1 knockin mouse, the tetO-hAIMP1 construct was cloned to contain human AIMP1 cDNA under the control of a minimal promoter from hCMV fused to the tetO sequence. This construct was subcloned into ROSA targeting vector (Soriano P's lab, New York, NY). The targeting vector was electroporated into mouse ES cells (E14TG2a), according to a previously reported procedure [25]. Correctly, targeted clones were screened by Southern analysis and were injected into C57BL/6 blastocysts for chimera generation. Germline

transmission of knockin allele was verified by PCR using ROSA locus specific primers. TRE-hAIMP1 mice were crossed to CAG-rtTA3 (Jackson Laboratories), Krt14-rtTA (Jackson Laboratories), or K14-Cre (Jackson Laboratories) with Rosa26-CAGs-LSL-rtTA3 (Jackson Laboratories) to generate systemic or skin-specific hAIMP1 inducible mice.

Generation of AIMP1 CKO mouse

For generation of conditional AIMP1 knockout, AIMP1 CKO targeting vector was cloned to contain floxed exon2 and Frt-Neo-Frt cassette with homologous arms (~3kb in each side) in pBR322. The targeting vector was electroporated into mouse ES cells and correctly targeted clones were screened by PCR analysis. Confirmed ES cells were injected into C57BL/6 blastocysts for chimera generation. Germline transmission of CKO allele was verified by PCR using the genotyping primers. AIMP1 fl/fl mice were crossed to K14-Cre (Jackson Laboratories) to generate skin-specific AIMP1 KO mice.

Hair depilation and peptide administration

For hair cycle induction, hair on the dorsal skin of 7 to 8-week-old mice was manually depilated to induce a new hair cycle after confirming that the skin had a

light pink color, which indicates that the HFs are synchronized at the telogen phase. For peptide treatment, 150 μL of peptides (20 nM) were topically applied to the shaved area once per a day. We use thioglycolate hair removal cream (Ildong Pharmaceutical, Seoul, Korea) for chemical depilation.

Western blotting

Primary HFSCs and DPCs were harvested with lysis buffer (25 mM Tris-HCl, pH 7.5, 100 mM NaCl, 5% glycerol, 0.5% Triton X-100, and 1 mM EDTA) containing 1X protease inhibitor tablet (Roche, Basel, Switzerland) and 1X phosphatase inhibitor tablet (Roche). The protein concentration was measured by the Bradford assay [26]. Whole-cell lysates were subjected to gel electrophoresis. Using semidry transfer, the proteins were transferred to polyvinylidene fluoride membranes. The membranes were immersed in 5% skim milk (BD Biosciences, Franklin Lakes, NJ, USA) for 30 min and then incubated with each primary antibody diluted in 1% skim milk. Primary antibodies used in this study were alkaline phosphatase (ALP; Santa Cruz Biotechnology, Dallas, TX, USA), beta-catenin (Cell Signaling Technology, Danvers, MA, USA), N-AIMP1 (Atlas Antibodies, Bromma, Sweden), C-AIMP1 (Novus Bio, Littleton, CO, USA), AKT (Cell Signaling Technology), phospho-AKT (Cell Signaling Technology), ERK (Cell Signaling Technology), phospho-ERK (Cell

Signaling Technology), FGFR2 (Abcam, Cambridge, UK), MMP2 (Thermo Fisher Scientific, Waltham, MA, USA) and tubulin (Novus Bio). After washing three times for 5 min each with 1x Tris-buffered saline containing Tween 20 (0.1% TBST), the membranes were incubated for 1 h with horseradish peroxidase (HRP)-conjugated secondary antibodies diluted in 1% skim milk and washed three times for 5 min each with 0.1% TBST. After incubation with western HRP substrate detection solution (Abcam) for a few minutes, immunoblot images were acquired.

In vivo patch hair reconstitution assay

Patch hair reconstitution assays were conducted in this study [27]. To isolate mouse dermal cells, the dorsal skin of C57BL/6 neonates was collected and incubated overnight with 1 mg/mL collagenase/dispase (Roche). The dermis and epidermis were separated by incubating the skin with 0.25% trypsin/10 mM EDTA in phosphate-buffered saline (PBS) at 37℃ for 15 min. The resulting epidermal and dermal cells were filtered through 70- and 100-mm cell strainers (BD Biosciences) respectively, and then centrifuged at 1500 rpm for 5 min. 3D-DPCs were combined with freshly isolated neonatal mouse epidermal cells (1×10^6 cells) and then subcutaneously co-implanted into the skin on the backs of 7-week-old female nude mice. After 2 weeks, the back skin was collected from the mice and reconstituted

HFs were quantified.

In vitro cleavage assay

AIMP1 and MMP2 (Novus Bio) were incubated in cleavage assay buffer (20 mM HEPES PH 7.4, 140 mM NaCl, 2 mM $CaCl_2$) for 2 h at 37℃. Next, 450 ng of ARP100 (Santa Cruz Biotechnology) and 300 ng of antibody (R&D Systems, Minneapolis, MN, USA) were used for each assay. Proteins were separated by sodium dodecyl sulfate polyacrylamide gel electrophoresis (SDS-PAGE) and subjected to immunoblotting.

Cell binding assay by fluorescence-activated cell sorting (FACS)

TN41 was biotinylated with an EZ-Link™ Sulfo-NHS-LC-Biotinylation kit (Thermo Fisher Scientific) following the manufacturer's instructions. DPCs (1.8×10^5) were cultured in 6-well plates containing Dulbecco's modified Eagle's medium (DMEM; Gibco BRL, Grand Island, NY, USA) with 10% fetal bovine serum (FBS), 1 ng/mL of FGF2, and 1% antibiotics for 24 h and then treated with the biotinylated 1 μM TN41 for 1 h. The cells were detached from by Accumax (Merck Millipore, Billerica, MA, USA) and washed twice with PBS containing 1% bovine serum albumin and 0.05% NaN_3 (FACS buffer). Cell were fixed by 4% paraformaldehyde for 10 min

then washed once with FACS buffer. The cells were incubated with phycoerythrin-conjugated streptavidin antibody (R&D Systems) diluted in FACS buffer for 30 min, and then washed twice with FACS buffer. Cell were resuspended in FACS buffer and then measured with a BD accuri^{TM} C6 plus flow cytometer (BD Biosciences)

Binding by enzyme-linked immunosorbent assay (ELISA)

A Maxisorp plate (Nunc, Roskilde, Denmark) was coated with recombinant proteins, AIMP1 (CureBio, Seoul, Korea) and FGF7 (Miltenyi Biotec, Bergisch Gladbach, Germany), and peptide, TN41 (GL Biochem, Shanghai, China) for 15 h at 4℃. For blocking, the coated plate was incubated with 5% bovine serum albumin in PBS. After blocking, FGFR2-flag recombinant protein (Origene, Rockville, MD, USA) was added to the plate for binding with the coated binding candidates. After washing with PBST (0.05% Tween-20), the plate was incubated with anti-flag M2 antibody (Sigma-Aldrich, St. Louis, MO, USA). The plates were further incubated with anti-mouse IgG HRP (Millipore). 1-Step Ultra TMB ELISA substrate (Thermo Scientific) was added to develop the signal. The absorbance at 450 nm was measured with a microplate reader (TECAN, Männedorf, Switzerland).

DPC proliferation assay

DPCs (1×10^4) were cultured in 96-well plates containing DMEM with 10% FBS, 1 ng/mL of FGF2, and 1% antibiotics for 24 h and then treated with TN41 at the indicated concentrations for 24 h. Cells were counted with a hemocytometer.

Isolation and culture of human HFs

Occipital scalp biopsy specimens were obtained during hair transplantation in male patients with androgenic alopecia. The Medical Ethical Committee of Kyungpook National University Hospital (Daegu, Korea) approved all described experiments. HFs were isolated from non-balding scalps as previously described method with minor modifications [28, 29]. Briefly, the subcutaneous fat portion of the scalp skin, including the lower HFs, was dissected from the epidermis and dermis. HFs were then isolated under a binocular microscope using forceps. Isolated hair follicles were maintained in Williams E media (Sigma) supplemented with 2 mM L-glutamine, 100 U/mL streptomycin, and 10 ng/mL hydrocortisone. Follicles were maintained in a humidified atmosphere of 5% CO_2 at 37℃.

Cell culture

HFSC were purchased from Cellprogen (Torrance, CA, USA). HFSCs before passage six were used. Outer root sheath and matrix cell were purchase from Sciencell research laboratories (Carlsbad, CA, USA). Cell culture were performed according to the manufacturer's instructions. The dermal papilla was isolated from the bulbs of dissected HFs, transferred onto plastic dishes coated with bovine type I collagen, and cultured in DMEM supplemented with 1% antibiotic-antimycotic solution and 20% heat-inactivated FBS at 37℃ in a humidified atmosphere containing 5% CO_2. These explants were incubated for several days, and the medium was changed every three days. Once subconfluent, the cells were harvested with 0.25% trypsin/10 mM EDTA in PBS, split at a 1:3 ratio, and then maintained in DMEM supplemented with 10% FBS.

TNF-α ELISA assay

RAW264.7 cells (2×10^4) were cultured in 24-well plates containing DMEM with 10% FBS and 1% antibiotics for 12 h and then treated with the purified protein at the indicated concentrations for 6 h. The media were harvested after centrifugation at 3,000 ×*g* for 5 min, and secreted TNF-α was measured using a TNF-α ELISA kit

(BD Biosciences) following the manufacturer's instructions.

Microarray analysis

Total RNA was extracted with an RNeasy Micro Kit (Qiagen, Hilden, Germany). The Illumina NextSeq500 array (San Diego, CA, USA) at the ebiogen (Korea, Seoul) was used. To analyze the GO terms with ≥2.0-fold increased or decreased gene clusters, the web-based Database for Annotation, Visualization and Integrated Discovery (DAVID) 6.7 was used (74). To extract reliable GO terms belonging to biological process, Fisher's exact test and multiple test correction ($P < 0.05$) were used.

AIMP1 secretion test

HFSCs were cultivated to 60% confluence in DMEM containing 10% FBS. After the cells were washed twice, they were transferred to serum-free DMEM for 2 h. WNT3a (R&D Systems), Noggin (Miltenyi Biotec), FGF7 (Sigma), SHH (Miltenyi Biotec), and transforming growth factor (TGF)-β2 (Thermo Fisher Scientific) were used to treat the cells, followed by incubation for 24 h. The culture media were

collected and centrifuged at 500 ×*g* for 10 min. The supernatants were centrifuged again at 10,000 ×*g* for 30 min to eliminate membrane organelles, and then the proteins were precipitated with 12% trichloroacetic acid and incubated for 12 h at 4℃. Pellets were obtained by centrifugation at 18,000 ×*g* for 15 min and neutralized with 100 mM HEPES, pH 8.0. Proteins in the pellets were separated by SDS-PAGE and subjected to immunoblotting.

Hematoxylin and eosin staining (H&E)

Paraffin sections were deparaffinized and then rehydrated. Frozen sections were removed from the optimal cutting temperature compound and stained with hematoxylin-eosin (Sakura FineTechnical Co., Ltd., Tokyo, Japan) for tissue histology analysis using an optical microscope.

Immunofluorescence staining (IF)

Paraffin sections were used for immunofluorescence analysis. Slides were incubated for 15 min at 60℃, and then immersed at xylene twice for 5 min for deparaffinization. Slides were soaked into 100% EtOH twice for 2 min, 95% EtOH twice for 1 min, and 80%, 70%, and deionized H_2O for 1 min for dehydration. Antigen

retrieval was performed by boiling the slides for 20 min in antigen unmasking solution (Vector Laboratories, Burlingame, CA, USA). Slide were removed from the microwave, cooled in buffer for 15 min, rinsed gently with running water for 5 min, and washed with PBS for 5 min. Nonspecific staining was blocked by incubation with CAS block (Life technology, CA, USA) for 30 min. Tissue sections were incubated with the primary antibody at 4℃ overnight and then washed 3 times with PBS containing 0.2% Triton X-100 (Sigma) (PBSTx). The following antibodies were used: CD34 (Abcam), Ki67 (eBioscience), beta-catenin (Abcam), LEF1 (Thermo Fisher Scientific), c-MYC (Abcam), KRT15 (Abcam), SOX9 (eBioscience), GFP (Invitrogen, Carlsbad, CA, USA), AIMP1, and glutamyl-prolyl-tRNA synthetase (EPRS). Sections were incubated with secondary antibodies conjugated with Alexa Fluor 488 or 594 (Invitrogen). After washing 3 times with PBSTx, 4′, 6-diamidine-2′-phenylindole dihydrochloride (Thermo Fisher Scientific) was added for nuclear counterstaining. Coverslips were mounted onto glass slides with fluorescent mounting medium (Biomeda Corp., Burlingame, CA, USA). All images were obtained by A1 confocal microcopy (Nikon, Tokyo, Japan).

Preparation of paraffin and frozen sections

For paraffin sections, mouse skin or human scalp skin was fixed in 10% formalin

solution at 4℃ overnight and then embedded in paraffin. Paraffin-embedded skin specimens were cut into 5-μm-thick sections. For frozen sections, mouse skin or human scalp skin was immersed in ice cold 4% paraformaldehyde in PBS (pH 7.4) and then irradiated in a 500-W microwave oven for three 30-s cycles at intervals and then kept on ice for 20 min. The fixed skin samples were embedded in optimal cutting temperature compound (Sakura FineTechnical Co., Ltd), snap-frozen in liquid nitrogen, and stored at -80℃. Frozen samples were cut in 10-μm-thick sections.

Results

AIMP1 protects against hair loss and aging

Aged C57BL/6 mice showed diffuse and symmetric patterns of hair loss on the back that typically became apparent on the dorsal-most area of the neck and trunk with the formation of a patchy or linear hair loss pattern and distal spreading toward the flanks [30]. Because hair loss in C57BL/6 mice normally becomes apparent at approximately 16 months after birth, we used 16-month-old mice for histological analysis of the HFs in the normal (Hair+) and hairless (HL) regions (Fig. 1A, yellow and red circles, respectively). As expected, the skin of the HL regions showed a significant decrease in HFs (Fig. 1A). HFSC aging in mice and humans causes stepwise miniaturization of HFs followed by hair loss [31]. To determine the functional relevance of AIMP1 in HF maintenance, we compared the expression levels of AIMP1 in the HFs between the normal and hairless regions by immunofluorescence staining and observed that the AIMP1 level was dramatically decreased in the bulge and secondary hair germ regions of hair follicles isolated from the hairless region (Fig. 1B). The fluorescence intensity (FL) of AIMP1 in Hair+

regions was twice higher than HL regions. In contrast, the expression level of EPRS, a component of the multi-tRNA synthetase complex together with AIMP1, was not changed between the two regions (Fig. 1B). These results suggest that AIMP1 has a specific function in maintaining HFs.

We also compared the AIMP1 levels in HFs from young (2 months old) and old (24 months old) mice (Fig. 1C). Histological analysis confirmed a significant decrease in HFs in the skins of the old mice (Fig. 1C). Immunofluorescence staining of AIMP1, but not EPRS, revealed a significant decrease in HFs isolated from old mice (Fig. 1D). We also compared the levels of the HFSC markers including SOX9 and keratin 15 (K15) by immunohistochemistry and observed deceases in these markers in old HFs (Fig. 1E, respectively). Interestingly, AIMP1 co-localized with these markers in the bulge cells of HFs (Fig. 1E), suggesting its potential function related to HFSCs.

To determine whether AIMP1 would play a role in HF maintenance, we generated HF specific AIMP1 depletion mice [AIMP1-K14 cre] and evaluated whether depletion of AIMP1 affected hair loss (Fig. 2A). The fl/fl homozygous AIMP1-K14 cre mice (6 months old) showed increased hair loss on the back and neck (Fig. 2B), and thinner hairs (Fig. 2C and 2D), suggesting that AIMP1 is required to maintain healthy hair. Unhealthy hairs are easily pulled off from the follicles because of the shortage of HFSC factors [32]; thus, we conducted a hair-pull test by applying an adhesive surgical tape and then peeling it off from the hair coat. More hairs were

removed from the skin of the fl/fl mice compared to from fl/+ mice, indicating that AIMP1-K14 cre mice hairs were released more easily than WT hairs (Fig. 2E). These data suggest that AIMP1 functions in part to ensure adequate adhesion of the bulge to prevent its loss and maintain the HF niche.

We next investigated whether AIMP1 stimulates hair growth *in vivo*. For this, we generated K14-AIMP1 conditional transgenic mice (cTg) in which AIMP1 expression could be induced in a skin-specific manner (Fig. 3A). We shaved the dorsal back of wild-type and AIMP1 cTg mice at postnatal day (PND) 49 when the second telogen normally takes place and observed hair cycle progression and regrowth at time interval between the two type mice under native conditions (Fig. 3B). In this manner, we could pinpoint the hair cycle stage according to the transition of skin color from pink (telogen) to grey (anagen) [33]. The cTg mice entered anagen, showing the next hair coat in a shorter time compared to in WT mice (Fig. 3C). A difference in hair regrowth from the dermis to the skin surface was also confirmed by hematoxylin and eosin staining of the skin (Fig. 3D). Immunofluorescence staining for the proliferation marker Ki67 revealed more Ki67-positive cells in the bulge of AIMP1 cTg mice at PND 70 (Fig. 3E). These results further support the positive role of AIMP1 in hair growth and the hair cycle.

We also generated systemically inducible AIMP1 transgenic mice (iTG) to gain insight into AIMP1 function. We confirmed generated mice by southern blotting,

western blotting, and immunohistology assay (Fig. 4A). We shaved the hair of AIMP1 iTG and WT mice at PND 49 and induced AIMP1 expression at PND 50 by doxycycline administration. Four weeks later, four AIMP1 iTg mice showed hair recovery over 70% of the depilated back skin area, while only one WT mice displayed a similar degree of recovery (Fig. 4B). Like skin-specific K14-AIMP1 cTg, AIMP1 iTg mice showed more Ki67-positive cells in the matrix region (Fig. 4C). Based on these results, AIMP1 promotes transition from telogen to anagen.

Fig 1. *In vivo* correlation of AIMP1 level with hair.

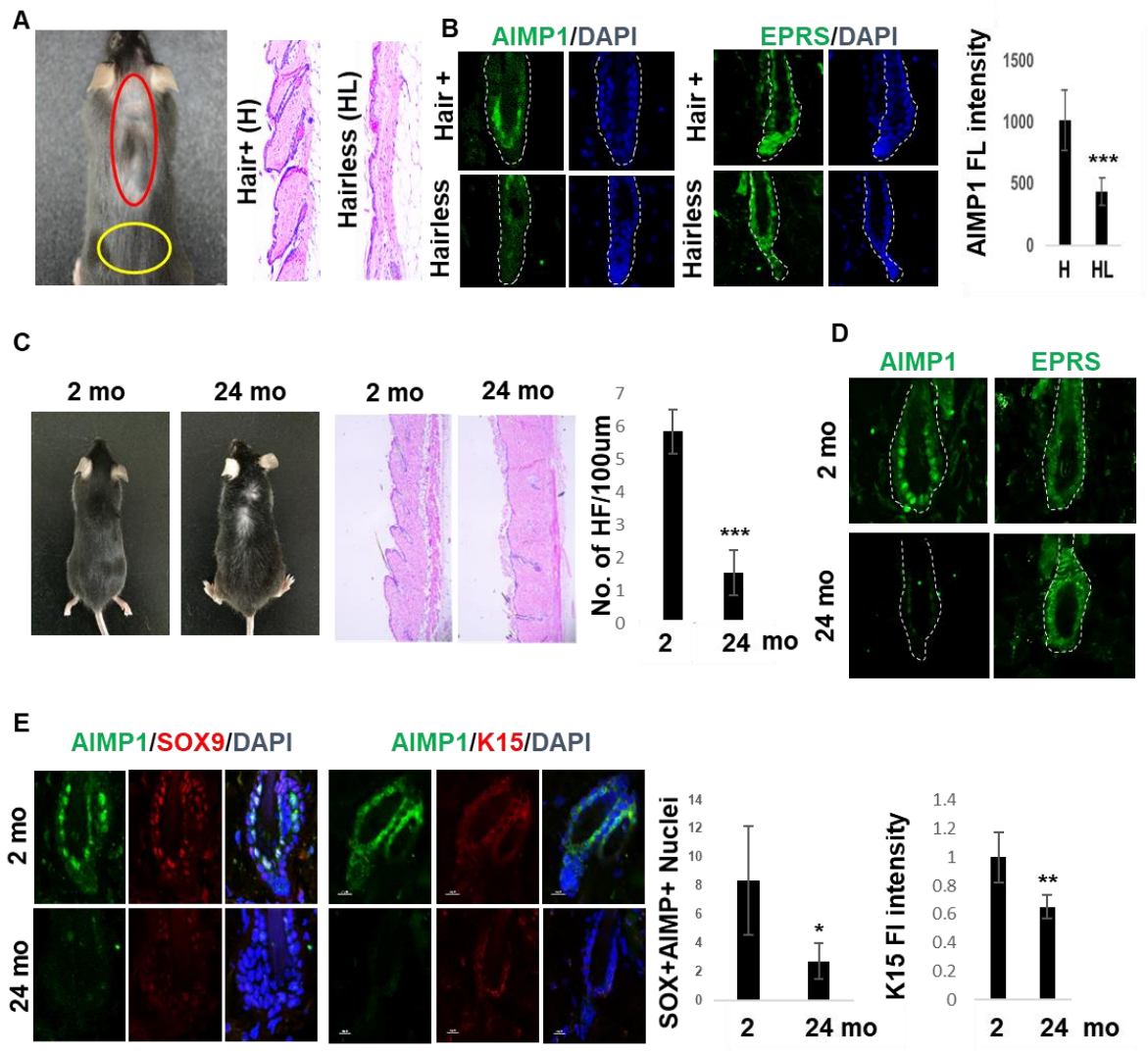

A. Image of C57BL/6 mouse (16 months). Representative histology of the dorsal skin from wild-type (WT) mice by hematoxylin and eosin stain at Hair+ (H) and Hairless (HL) areas. Red circle: hairless region, Yellow circle: hair+ region.

B. Immunofluorescence images with AIMP1 and EPRS at HL and H areas. Quantitative analysis of fluorescence intensity AIMP1 in bulge areas. Several HFs

(>5) from each group were examined. N = 3 mice for each group.

C. Representative mice image at 2 months (2 mo) and 24 months (24 mo) aged mice. Representative histology of the dorsal skin from 2 mo and 24 mo mice by hematoxylin and eosin stain. Hair follicle number per 100um was counted.

E. IF images at 2 and 24 months mice for AIMP1, SOX9 and K15. Quantitative analysis of the number of AIMP1+ and SOX9+nuclei in bulge cells 2 and 24 months mice. Quantitative analysis of fluorescence intensity K15 in bulge areas. ; several HFs (>5) were examined.

Error bars mean STD. *: P<0.1, **: P<0.01 and ***: P<0.001 (Student's t test).

Fig 2. Hair defects of skin specific AIMP1 depletion mouse.

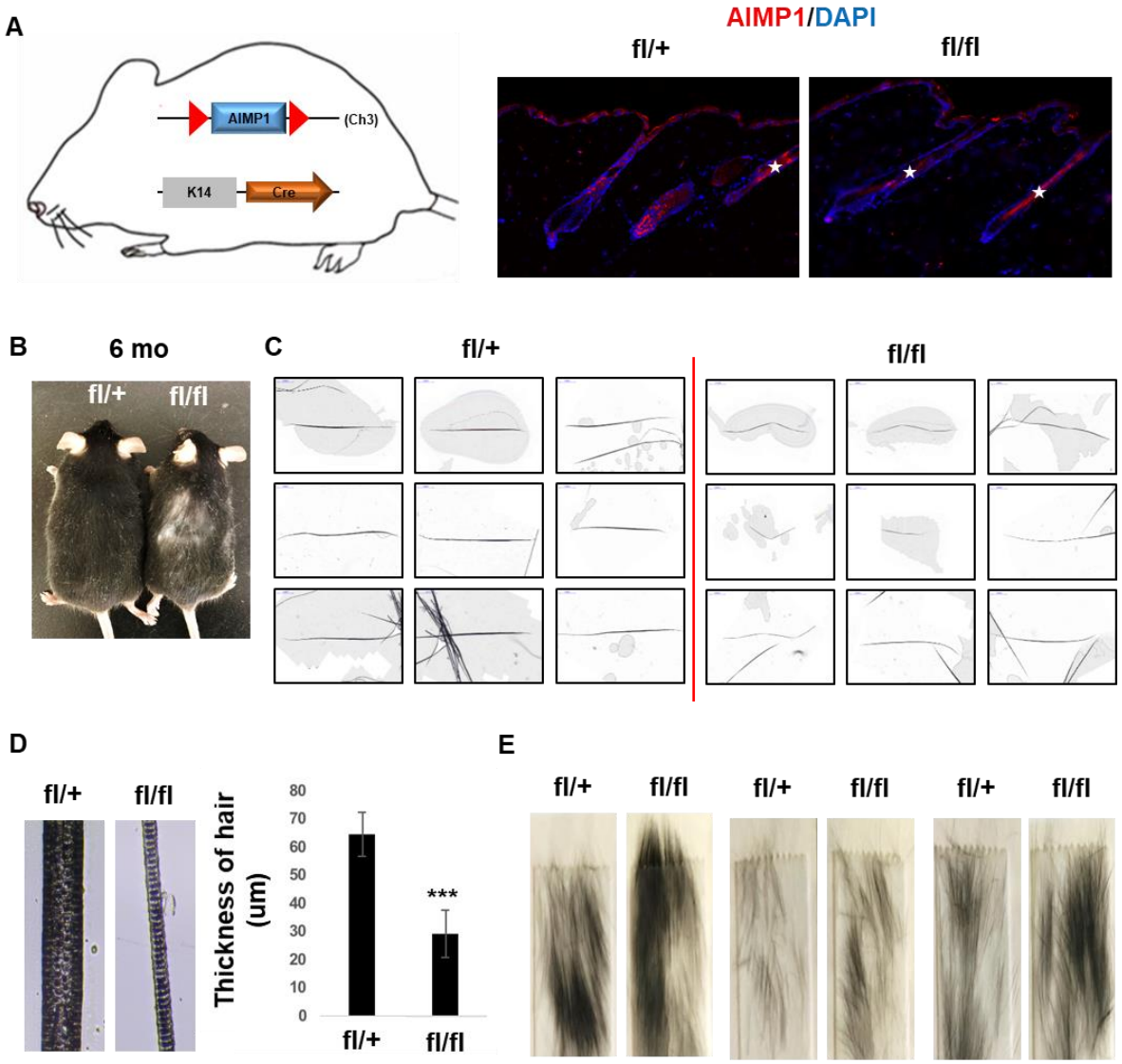

A. Shema of generating skin specific AIMP1 conditional KO mouse. Validation of AIMP1 deletion in epithelial cells in skin specific AIMP1 conditional KO mouse model by immunofluorescence. Skin tissue section from KRT14-cre; AIMP1fl/+ (fl/+) or KRT14-cre; AIMP1fl/fl (fl/fl) mouse were immunostained with anti-AIMP1 antibody. White star: Auto fluorescence

from hair shaft.

B. Images of fl/+ and fl/fl mice at 6 month (6mo). fl/fl mouse showed hair defect.

C. Mice hair from fl/+ and fl/fl mice. Hair from each mice were mounted on the slide glasses.

D. Measurement of hair thickness from fl/+ and fl/fl mice. Nine HFs were examined. N=3 mice for each group. Error bars mean STD. ***: $P<0.001$ (Student's t test).

E. Images of pulled out hair from fl/+ and fl/fl mice.

Fig 3. Effect of skin specific overexpressed-AIMP1 on hair growth.

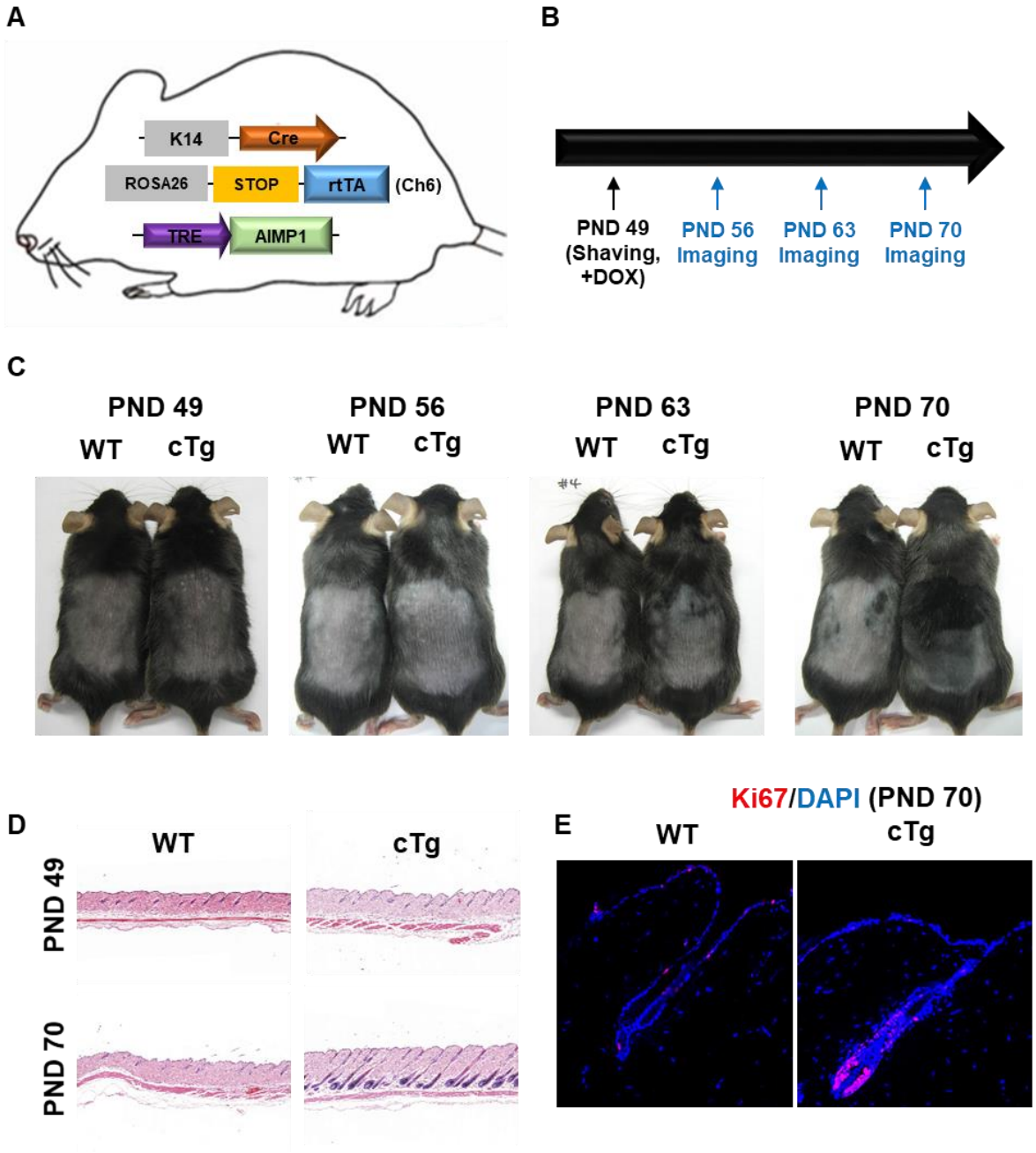

A. Schematic diagram of skin-specific hAIMP1 inducible mouse model.

B. Experimental design for analysis of hair growth. WT and K14-AIMP1 cTg mice were shaved at postnatal 49 days (PND 49). 1.6mg/ml of Doxycycline contained

water was supplied at the same day. Images were obtained at PND 49, PND 56, PND 63 and PND 70.

C. Images of WT and K14-AIMP cTg mice at PND 49, PND 56, PND 63 and PND 70.

D. Representative histology of the dorsal skin from WT and K14-AIMP1 cTg mice by H&E stain at PND 49 and PND 70.

E. IF images with Ki67 of K14-AIMP1 cTg and WT mouse.

Fig 4. Effect of systemic AIMP1 overexpression on hair growth.

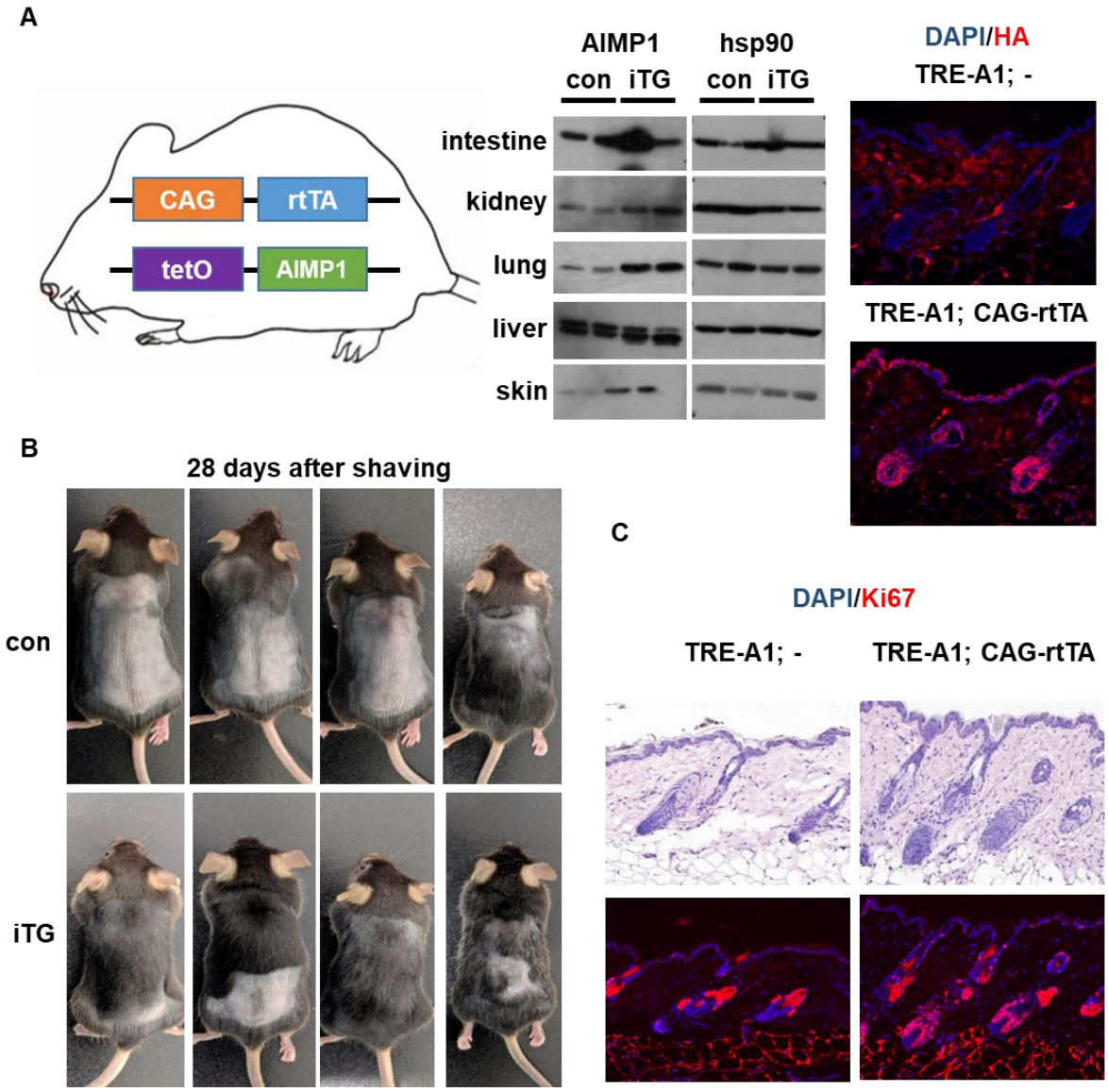

A. Schematic diagram of systemic-hAIMP1 inducible mouse model, CAG-rtTA; tetO-hAIMP1 (iTG). Characterization of iTG mice by southern, western blotting and immunohistology assay.

B. Mice image of WT and iTG at 28 days after shaving.

C. H&E and IF images with Ki67 of iTG and WT mouse.

Effect of AIMP1 peptide treatment on hair growth

To characterize the functional domain of AIMP1, we prepared four peptides based on a previous report (Fig. 5A) [19]. Among them, the N-terminal peptide of AIMP1, N192 (aa 1–192), was previously shown to stimulate collagen synthesis, fibroblast proliferation, and wound healing [19]. TN41 was shown to enhance the proliferation of human bone marrow-derived MSCs by accumulating beta-catenin via FGFR2-mediated activation of ERK and AKT [20]. To determine the peptide region active in hair recovery, we used the four selected peptides of AIMP1 to treat the dermal papilla, outer root sheath, hair matrix, and HFSCs, which are known to play important roles in hair biology, and analyzed the accumulation of beta-catenin from each cell, as beta-catenin is a key molecule in hair growth and maintenance in the HF microenvironment [34-37]. Full-length AIMP1 (FL), N192, and TN41, but not C120 (aa 193-312), elevated the beta-catenin level in human DPCs at 20 nM (Fig. 5B). In contrast, AIMP1 FL and TN41 did not increase the beta-catenin level in the hair matrix, outer root sheath, or HFSCs (Fig. 5C, respectively). We then examined the *in vivo* effect of AIMP1 FL and TN41 on hair regrowth. We depilated mouse back skin (PND 49) with clippers and then completely removed the remaining hair with cream. The mice treated with AIMP1 FL and TN41 showed faster hair recovery compared to the control group, further validating their effects on DPCs (Fig. 5D).

Interestingly, AIMP1 FL, but not TN41, caused some signs of inflammation such as skin swelling, perhaps because of the known inflammatory activity of AIMP1 FL [15, 38]. To confirm this possibility, we treated Raw264.7 cells with the four different AIMP1 peptides and monitored the secretion of TNF-α, the signature cytokine of inflammation [39]. AIMP1 FL and N192, but not TN41 and C120, induced the secretion of TNF-α as lipopolysaccharide (Fig. 5E) [10, 38, 39]. To investigate hair growth effect of AIMP1 peptide, excluding inflammatory function, we decided to use TN41 in the following experiments [40-42].

To determine *in vivo* effect of TN41 on hair growth, we shaved the back hair of C57BL/6 mice with clippers and applied vehicle and TN41 to the left and right sides of the shaved region, respectively (Fig. 6A). After treatment with TN41 every other day for 4 weeks, the TN41-treated regions showed more rapid hair recovery compared to the vehicle-treated regions (Fig. 6B). These results indicate that TN41 can facilitate the transition of the telogen to anagen phase so that HFs can initiate the anagen phase earlier for active hair growth. We performed an immunohistology assay to identify the expression of Ki67 in the bulge region. Higher staining intensity of Ki67 was observed on the secondary hair germ of the TN41-treated mice at post-depilation day (PD) 6, and the Ki67 signal was spread out from the area of the CD34-positive stem cells (Fig. 6C and 6D).

To determine the effect of TN41 on hair growth rate, we treated chemical-depilated mice with TN41 (20 and 100 nM), and minoxidil (MNX), which is known increase hair growth rate via vasodilatation, resulting in greater nutrient feeding to DPCs [43, 44], and compared hair recovery. The skin of the vehicle-treated mice entered anagen phase at PD 12, when hair regrowth from the skin was not yet apparent. However, hairs were observed on the mouse back skin in both groups of TN41-treated mice as well as in the MNX-treated group (Fig. 6E). To confirm this result, we examined the expression levels of Ki67 and c-Myc in hair follicles by immunofluorescence staining. High expression of Ki67 and c-Myc was observed in the hair germ region and DPCs (Fig. 6F). We also used TCF/LEF1-GFP mice and treated them with TN41. Because TCF/LEF1 is a known target gene of beta-catenin, we used TCF/LEF1-GFP transgenic mice in which TCF/LEF1 was expressed as a fusion protein with GFP to evaluate the effect of TN41 on inducing beta-catenin. We depilated the TCF/LEF1-GFP mice with clippers followed by treatment with vehicle and TN41 on the left and right sides of the back, respectively. Four days after treatment, we evaluated the TCF/LEF1-GFP levels in the hair bulge by immunofluorescence staining using an anti-GFP antibody and observed that the GFP level was significantly higher in the TN41-treated mice than in the vehicle-treated mice, suggesting that TN41 induced beta-catenin in the HFs (Fig. 6G). These results indicate that TN41 induces beta-catenin, leading to the expression of c-Myc

and TCF/LEF1 for stimulating the proliferation of the secondary hair germ and DPCs for hair growth.

Based on the positive activity of TN41 in the transition from telogen to anagen phase and hair growth rate, we hypothesized that deletion of AIMP1 would cause a defect in hair growth. We generated skin-specific AIMP1 knockout mice and examined the effects of AIMP1 depletion on hair recovery after depilation at PND 49. While hairs of the WT mice were fully recovered at 5 weeks later, AIMP1 deletion mice showed slower hair growth (Fig. 7B). In the first week, the areas of hair growth on the back among all tested groups were similar (Fig. 7A and 7B). However, after five weeks later, the hair-recovered areas of the WT mice were approximately five-fold higher than those of the skin-specific AIMP1 knockout mice (Fig. 7B). Signals for beta-catenin and LEF1 in the HFs appeared at PD 9 and PD 6 in the WT mice, respectively, whereas neither signal was observed in skin-specific AIMP1 knockout mice until PD 20 (Fig. 7C). Additionally, the TN 41-treated group showed earlier hair growth and 2-fold faster hair recovery rate compared to the untreated group in both WT and knockout mice (Fig. 7A and 7B). These results suggest that TN41 stimulates the transition from telogen to anagen phase and hair growth rate.

Because the expression level of AIMP1 showed a positive correlation with HFSC markers (Fig 1E), we checked whether skin-specific depletion of AIMP1 would

affect the stem cell fate by immunofluorescence staining of HFs. While hair growth was significantly retarded by AIMP1 depletion (Fig. 7A and 7B), the staining intensities of the stem cell markers CD34 and K15 were only slightly changed (Fig. 7D), suggesting that depletion of AIMP1 in the HFSCs would not significantly affect the stem cell population.

To examine whether TN41 affects the normal hair cycle, we subjected the mice to chemical depilation so that the mice synchronously entered the first anagen phase and compared the times required to reach the next telogen phase between the TN41-treated and non-treated groups. The two groups entered the telogen phase at three weeks after depilation (Fig. 7E), suggesting that TN41 did not alter the length of the hair cycle although it facilitated hair growth.

Fig 5. : Determination of the peptide region of AIMP1 responsible for the hair growing activity.

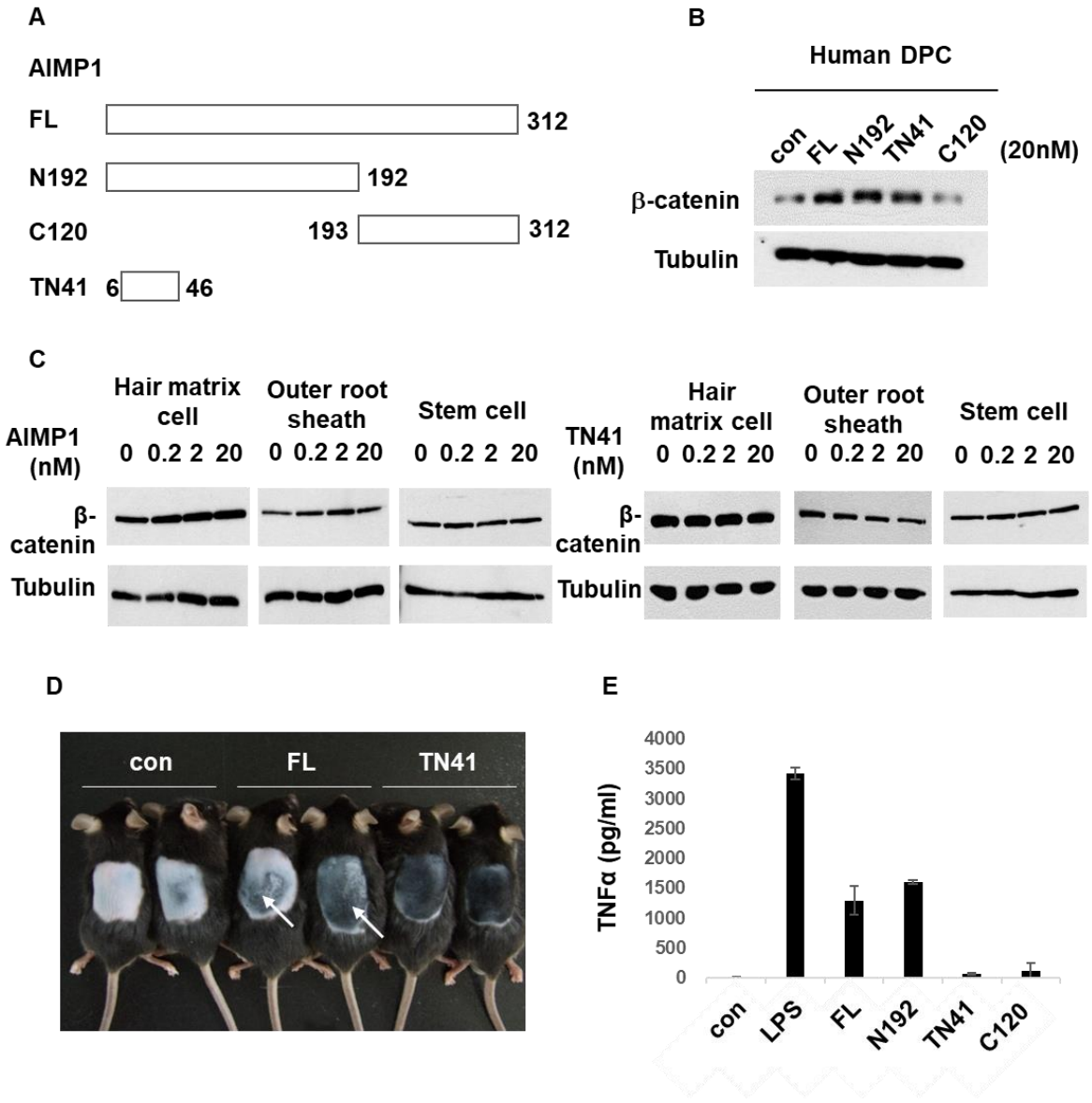

A. Fragments of AIMP1. FL: Full length AIMP1, N192: 1aa-192aa of N-terminal IMP1, C120: 193aa-312aa fragment of C-terminal AIMP1, TN41: 6aa-46aa of N-terminal AIMP1.

B. DPC was treated with FL, N192, TN40 and C120 (Each 20nM). Western blot performed with beta-catenin antibody.

C. Hair matrix cell, outer root sheath cell and HFSC were treated with FL and TN41 (Each 20nM). Western blot performed with beta-catenin antibody.

D. Dorsal area of WT mouse back hair were shaved at PND 49. Back skin hair were completely removed by hair removal cream. FL (100nM) and TN41 (100nM) were treated for 2 weeks. White arrows indicate inflammation.

E. TNF- α secretion was detected by ELISA. Raw 264.7 cell was treated with FL, LPS, N192, TN40 and C120 (LPS: 1ug/ml, Each fragments: 20nM). Error bars mean STD.

Fig 6. Effect of AIMP1 peptide treatment on hair growth.

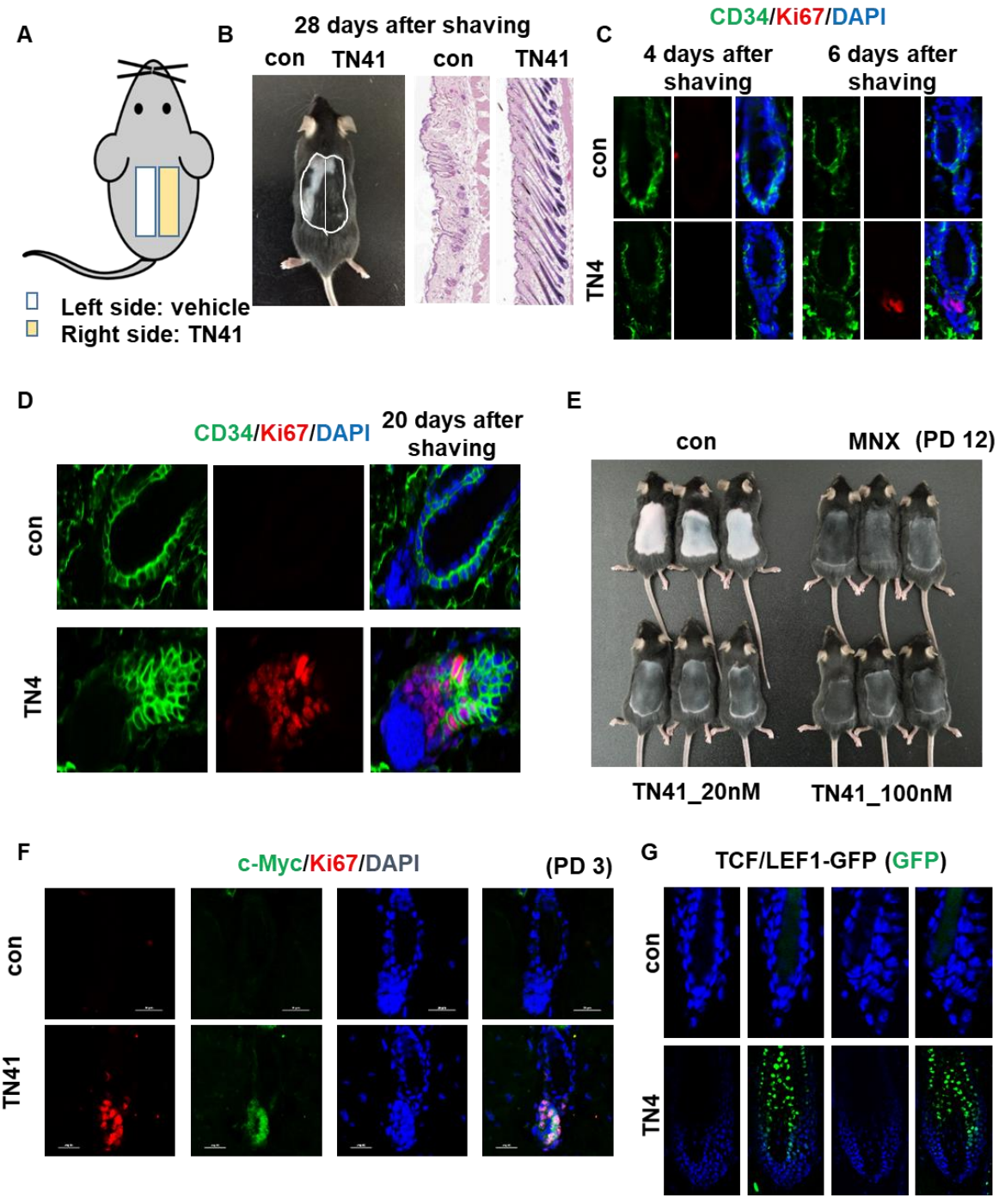

A. Experimental design for analysis of hair growth.

B. Mouse back hair were shaved at PND 49. Image was taken after 28 days from

shaving. Left half of back skin was treated with vehicle (carbomer). Right half was treated by TN41 in carbomer (100nM of TN41). Representative histology of the dorsal skin from WT mice by H&E stain.

C. IF images with CD34 and Ki67 at 4 and 6 days after shaving.

D. IF images with CD34 and Ki67 at 20 days after shaving.

E. Mouse back hair were shaved at PND 49. Back skin hair were completely removed by hair removal cream. Image was taken after 12 days from shaving. 3% Minoxidil (MNX), TN41 (20 and 100nM TN41).

F. IF images at PD 3 for c-Myc and Ki67.

E. Shaved back skin of TCF/LEF1-GFP mouse was treated with 100nM of TN41. IF images of TCF/LEF1-GFP for GFP at PD 4.

Fig 7. Effect of AIMP1 peptide treatment on hair growth of skin specific AIMP1 deletion mouse.

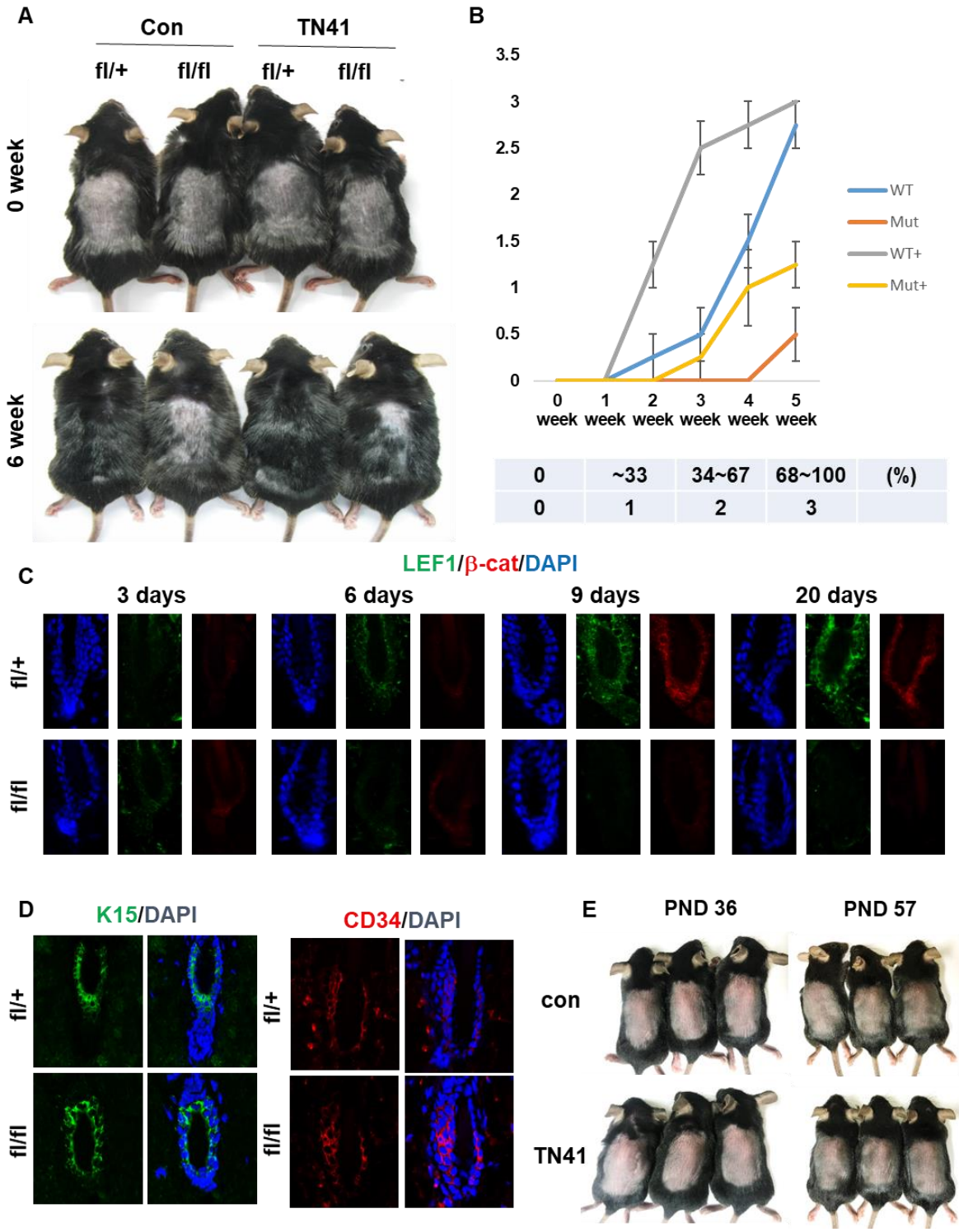

A. Mice image of WT and K14-AIMP1 cre mouse at 0 and 6 weeks. Mice shaved at PND 49. Mice were treated with 150ul of TN41 or vehicle once a day.

B. Hair growth was measured at 0, 1, 2, 3, 4 and 5 weeks by Image J program. WT: fl/+, Mut: fl/fl, +: 100nM of TN41, -: non-treated. Error bars mean SEM. Hair growth scoring; 0-25%: 0, 25-50%: 1, 50-75%: 2, 75-100%: 3. N = 4 mice for each group.

C. IF images with beta-catenin and LEF1 at 3, 6, 9 and 20 days after shaving.

D. IF images for K15 and CD34 from fl/+ and fl/fl mice.

E. Hair cycle analysis assay. Mice were shaved completely by chemical depilation at telogen and observed to next telogen. N=3 mice for each group.

Mechanism of AIMP1 peptide in hair growth

A previous report showed that AIMP1 acts as a signaling molecule or an intracellular functional molecule [45, 46]. Mice to which TN41 had been applied showed rapid hair growth, and thus we first confirmed whether TN41 functions as a signaling molecule (Fig. 6). AIMP1 was enriched in the bulge with an expression pattern correlated with HFSCs (Fig. 1); thus, we evaluated the secretion of AIMP1 from HFSCs. We examined the regulation of AIMP secretion by treating HFSCs with the effector molecules; FGF7, Noggin, SHH, TGFβ2, and WNT3a. We observed cleaved AIMP1 approximately 20 kDa in size in the WNT3a-treated supernatant (Fig. 8A). The cleavage form of AIMP1 was detected with an N-terminal-specific AIMP1 antibody, whereas the C-terminal-specific antibody did not detect the AIMP1 peptide. To determine whether the detected peptide originated from AIMP1, we knocked down AIMP1 with an AIMP1-specific small interfering RNA. The secreted AIMP1 fragment decreased dramatically following treatment with short interfering RNA for AIMP1 (Fig. 8B). These data indicate that cleaved AIMP1 is secreted from stimulated HFSCs by WNT3a. Recently, a database-based peptide library was used to identify cleaved site of proteins [47]. Amino acids 188-205 of AIMP1 were predicted as the cleavage site and a candidate target of matrix metalloproteinase 2

(MMP2). The cleaved peptide contained 192 residues and had a predicted molecular weight of approximately 20 kDa. To determine whether AIMP1 is a real target of MMP2, we conducted an *in vitro* cleavage assay. MMP2 levels of 10–100 ng cleaved AIMP1. The cleaved form of AIMP1 was not observed after MMP2 was blocked with an inhibitor and antibody (Fig. 8C). The cleaved peptide was identified by mass spectrometry analysis. The peptide sequence of the AIMP1 fragment was found to originate from the N-terminal sequence (amino acids 1–205) of AIMP1 (Fig 8D). These data indicate that these AIMP1 sequences are targets of MMP2 and that the cleaved peptide of AIMP1 is secreted from HFSCs, supporting that N192 and TN41 are biologically valid.

We already know that beta-catenin in DPCs was accumulated by FL, N192, and TN41 (Fig. 5B). To identify the target cells of truncated AIMP1 *in vivo*, we used TN41 to treat the mouse back skin and tested the expression level of LEF1 in the DPC. TN41-treated mice showed higher expression of LEF1 on the DPC. This data revealed a functional target cell of secreted AIMP1 via *in vitro* and *in vivo* analysis (Fig. 9A). DPCs were treated with TN41 for 24 h and cell number was counted. The number of cells treated with DPCs was higher than non-treated DPCs (Fig. 9B). Additionally, the beta-catenin level of DPCs was increased by TN41 as concentration and time were increased (Fig. 9C). Next, we checked the alkaline

phosphatase (ALP) to determine whether DPCs were active [48–52]. ALP expression was increased following treatment of the cells with TN41 and the ALP level was increased from 4 to 24 h after treatment (Fig. 9D). ALP expression reached a maximum following treatment with 20 nM TN41, and then decreased at higher treatment concentrations (Fig. 9D). Thus, another feedback mechanism controls ALP in DPCs depending on the AIMP1 levels.

To gain insight into the underlying mechanism of AIMP1 in regulating beta-catenin, we performed western blot analysis. According to a previous report, the N-terminal region of AIMP1 induces beta-catenin in human bone marrow-derived MSCs via FGFR2-mediated activation of AKT and ERK [20]. Phosphorylation of AKT at residue 308 gradually increased in a time-dependent manner. Phosphorylation of ERK showed a similar pattern as AKT (Fig. 9E). Both proteins were phosphorylated before beta-catenin was induced, as beta-catenin is regulated by ERK and AKT.

Next, we confirmed whether FGFR2 is a functional receptor of TN41 in DPCs. We checked binding of AIMP1 with FGFR2 by ELISA. Binding affinity of AIMP1 is higher than FGF7, which was known as the ligand of FGFR2 (Fig. 9F). Moreover, binding of AIMP1 with DPC also significantly decreased when FGFR2 was reduced by small interfering RNA for FGFR2 (Fig. 9G, FGFR2#2 and FGFR2#4, we used #2 of small interfering RNA for FGFR2 for further experiments). Proliferation of DPC was not increased by TN41 when FGFR2 was blocked with inhibitor and small interfering

RNA (Fig. 9B). TN41 increased the phosphorylation level of both kinases; however, neither kinase was phosphorylated by TN41 when FGFR2 was decreased by short interfering RNA for FGFR2 (Fig. 9H). Beta-catenin accumulation was also decreased when FGFR2 was knocked down (Fig. 9H). TN41 increased the stability of FGFR2, providing a greater opportunity for FGFR2 to be phosphorylated (Fig9. H and I). Next, we confirmed that phosphorylation of ERK and accumulation of beta-catenin were altered by the FGFR inhibitor. Phosphorylation of ERK was upregulated by TN41, while the phosphorylated form of ERK was gradually decreased with the concentration of BGJ398 (Fig. 9J). Beta-catenin was also accumulated by TN41, but not when BGJ398 was used to block FGFR2 (Fig. 9J).

Fig 8. N-terminal of AIMP1 is cleaved by MMP2 and then secreted from HFSC

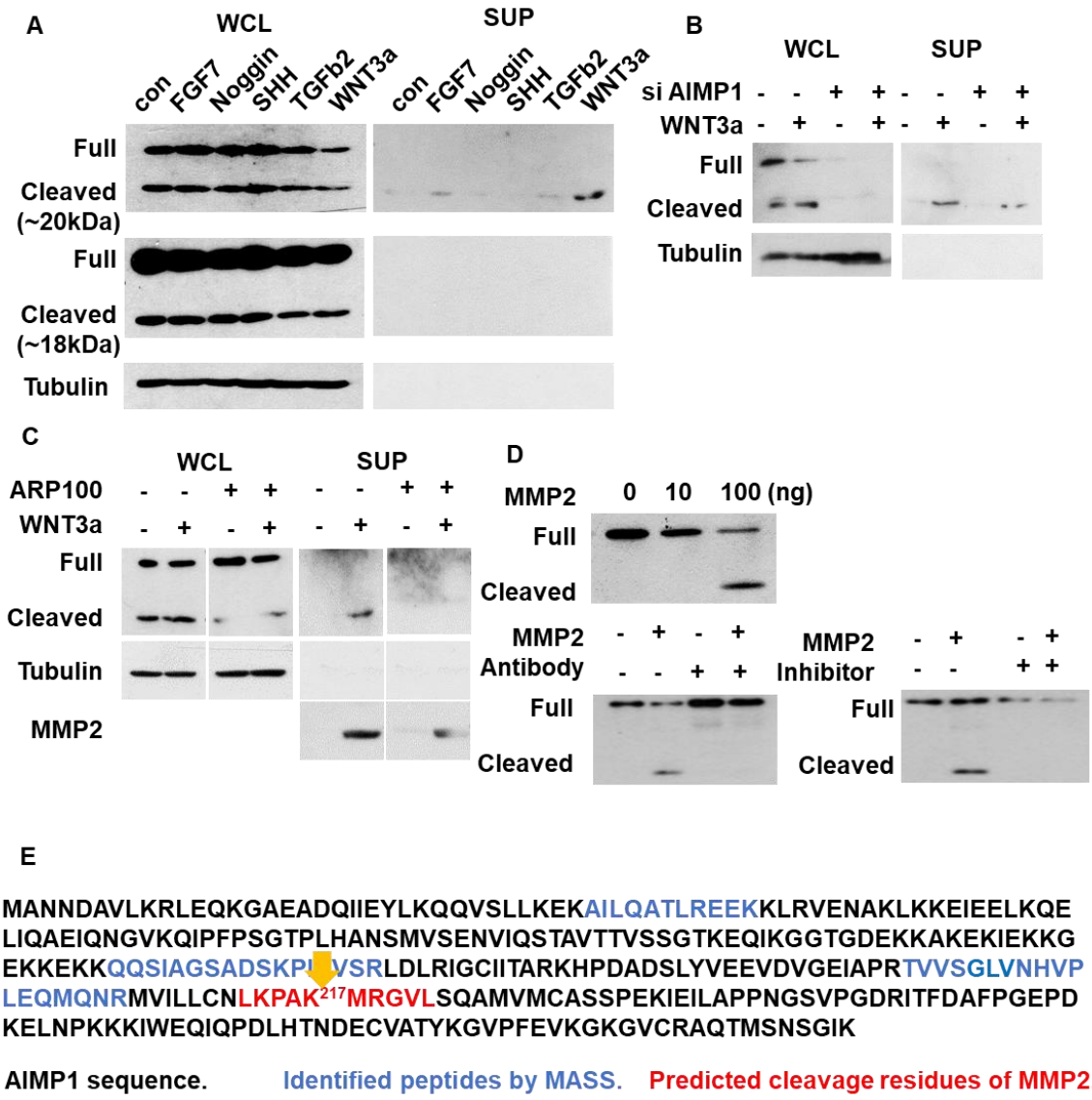

A. After serum starvation for 2 h, HFSC were treated with indicated molecules. Cells and supernatant (SUP) were harvested after 24 h. Western blot performed with N-terminal and C-terminal specific AIMP1 antibody. WNT3a: 200ng/ml, FGF7: 100ng/ml, Noggin: 200ng/ml, TGFb2: 10ng/ml, SHH: 200ng/ml

B. 10 pmol of si AIMP1 was transfected into HFSC for 48 h before doing secretion

assay. After serum starvation for 2 h, HFSC were treated 200ng/ml of WNT3a for 24 h. Western blot performed with N-terminal specific AIMP1 antibody.

C. MMP2 and GST-AIMP1 were co-incubated at 37℃ for 2 h. Western blot performed with GST antibody. MMP2: 0-100ng, AIMP1: 400ng, MMP2 antibody: 300ng, ARP100: 450ng.

D. N-terminal peptide was identified by mass spectrometry analysis. Blue: identified peptide, Red: 192aa residue.

Fig 9. HFSC secretes N-terminal of AIMP1 for activation of DP through FGFR2 receptor.

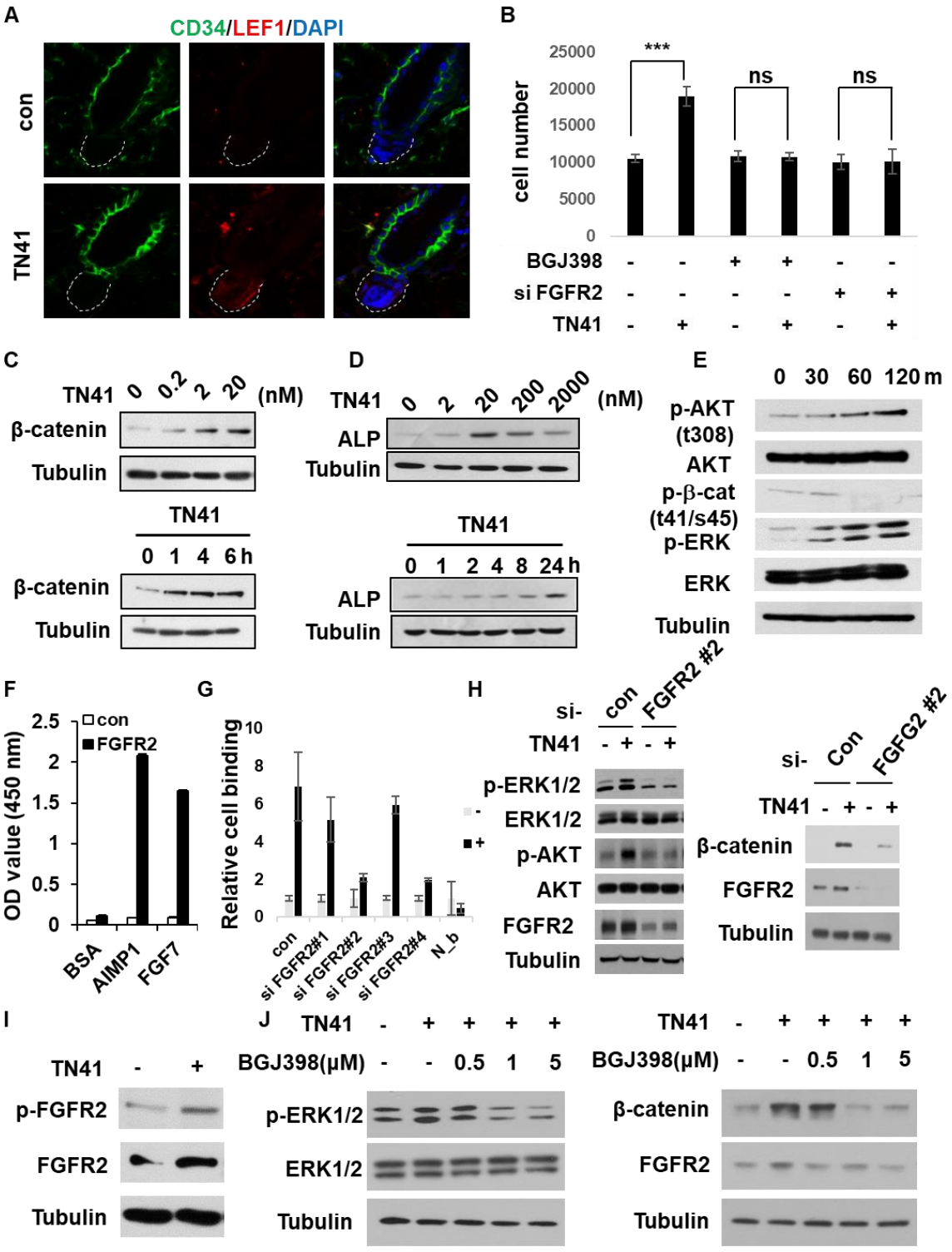

A. IF images with CD34 and LEF1. Mice were shaved at PND 49 and treated with TN41 (100nM).

B. 10000 numbers of DP cells were seeded into 96 well. Cell number was counted after 24 h (TN40: 20nM, BGJ398: 1uM, si FGFR2: 10 pmol). Error bar mean STD, ***: P<0.001 (Student's t test), ns: not significant.

C. TN41 was administered at DPC with indicated concentration and time. Western blotting was performed for beta-catenin.

D. TN41 was administered at DPC with indicated concentration and time. Western blotting was performed for alkaline phosphatase.

E. 20nM of TN41was added to DPC for the indicated time. Cell extracts were harvested and blotted with specific antibodies.

F. Identification of binding between AIMP1 and FGFR2 by ELISA.

G. FACS analysis for binding of AIMP1 with DPC. Biotinylated TN41 were incubated with DPC and FACS was performed with streptavidin antibody. N_b: Non-biotinylated TN41.

I. Activation of FGFR2 was identified by phosphorylation of FGFR2.

J. FGFR2 mediated phosphorylation of ERK and accumulation of beta-catenin were eliminated by FGFR2 inhibitor.

Effect of AIMP1 peptide on human HFs

We found that AIMP1 is functional protein that can regulate hair homeostasis of the cellular level and in mice. To identify the positive function of AIMP1 in human HFs, we performed a HF elongation assay. Human scalp HFs were isolated and cultured in the absence or presence of TN41. After six days, we measured the length of the HFs. TN41-treated human HFs showed approximately 30% greater elongation than non-treated HFs (Fig 10A). Next, we evaluated human HF proliferation in an immunohistology assay. Additionally, the number of Ki67-positive matrix keratinocytes around the DP was dramatically increased in TN41-treated HFs (Fig. 10B). Next, we performed a patch assay to determine whether TN41 can induce neogenesis of HFs by activating human DPCs. 3D-cultured human DPCs were treated with TN41 for 4 h and then transplanted onto the nude mice back skin. As expected, hair induction was achieved when TN41-treated human DP spheres (100 spheres; 10^6 cells) and mouse epidermal cells (10^6 cells) were co-transplanted (Fig. 10C). However, no hair induction was observed when implanting non-treated human DP spheres in combination with mouse epidermal cells. These data suggest that AIMP1 induces human HF formation by activating human DPCs, which leads to hair growth from balding skin.

Next, we compared the gene expression profiles of non-treated and TN41-treated DPC using microarrays. Numerous genes were found to be differentially

expressed. The top 50 up-regulated and down-regulated genes are summarized in Table 1 and 2. Interestingly, WNT10b was highly upregulated by TN41. WNT10b is well-known to promote the growth and regeneration of HFs via a canonical WNT signaling pathway [53, 54]. Moreover, COL17A1 was upregulated by 8.467-fold by TN41 and is a critical molecule for HFSC maintenance, DNA damage mediates the proteolysis of COL17A1 which triggers HFSC aging, characterized by the loss of stemness signatures and by epidermal commitment. Damaged HFSCs are cyclically eliminated from the skin through terminal epidermal differentiation, thereby causing HF miniaturization [31] (Table 1). Secreted Frizzled-related protein 4 (sFRP4) is a WNT inhibitor that is downregulated by TN41 (Table 2). SFRP4 inhibits HF regeneration [55]. We derived a molecular signature of genes >2x up-/downregulated in TN41-treated DP relative to the non-treated DP and used bioinformatics analysis to classify these genes. We found that the DPC was transcriptionally dynamic following treatment with TN41 (Fig. 10D) [56]. Notably, the transcription of genes within the "extracellular signal" category (blue box) was progressively enhanced; these genes contain transcripts encoding putative hair cycle stimulating factors (Fig. 10D). Further analyses revealed elevated expression of 42 of these DP genes in the signaling category (Fig. 10E). WNT 2/10b may promote HF growth and development [53, 54, 57]. Additionally, WNT16 activates human keratinocyte proliferation and differentiation via a beta-catenin-independent non-

canonical WNT transduction pathway [58]. DKK3 and SFRP4 are potent inhibitors of the WNT signaling pathway [55, 59, 60]. Elevated WNT genes and decreased inhibitory genes of WNT suggest that the DPC was activated by TN41 (Fig. 10E and 10F). FGF7 and its relative FGF10 were among the DPC signature genes elevated by TN41 (Figures 10E and 10F). The FGF7/FGF10 expression in the DPC coincided with an increase in the mitogen-activated protein kinase pathway (Fig. 9E) [56]. Combined with the results of previous studies, this suggests a paracrine role for FGF7/10 signaling in epidermal wound repair and hair growth [61-63]. FGFR2 showed the same trend and agreed with previous data (Fig. 9H and 9I). FGF18 showed higher DP expression on the TN41-treated DPC compared to on the non-treated DP. The trend in FGF18 was consistent with its anagen-inducing effects on DPCs [64]. In contrast, FGF5 showed an opposing trend, which was consistent with its growth-inhibitory effects on DPCs [65].

Fig 10. Effect of AIMP1 peptide on human hair follicle.

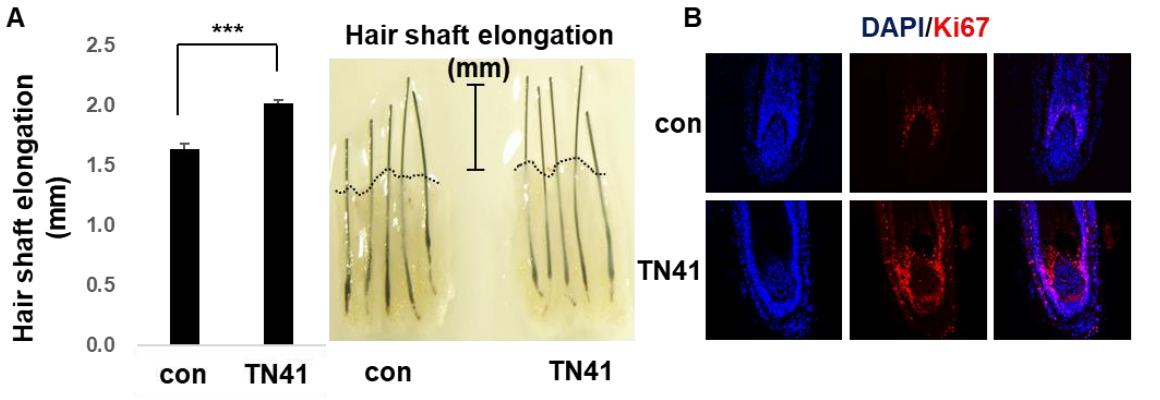

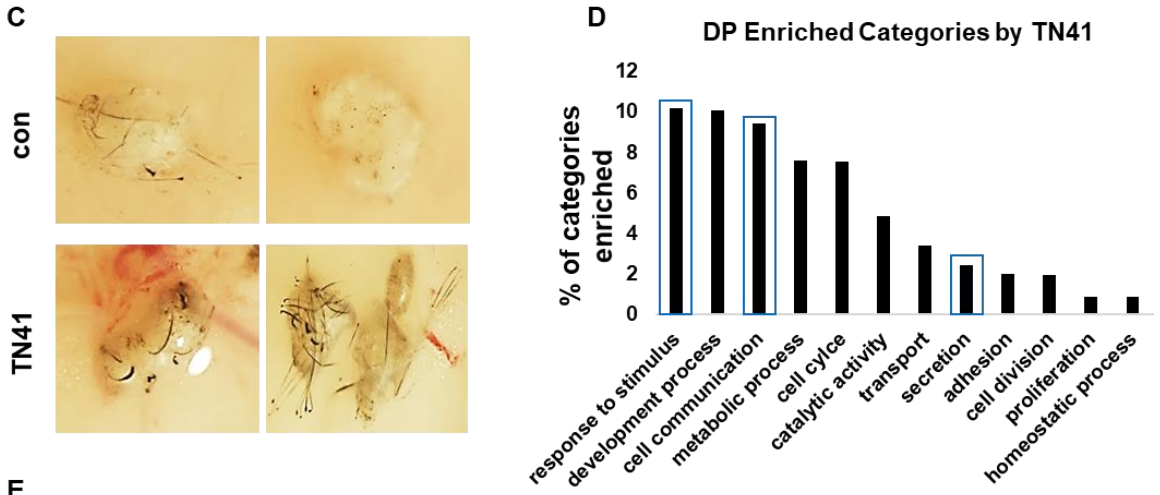

E

Gene	Fold↑	Gene	Fold↑
RNF43	13.650	MAGI2	2.702
WNT10B	12.832	BSN	2.587
TRHDE	7.083	PCDHB9	2.529
ACHE	6.672	CD24	2.504
DLGAP1	5.654	TRPV1	2.500
HRH4	4.612	PTPRN	2.479
ROR1	4.104	EFNA1	2.464
PCDHB5	4.069	GNRH1	2.390
STAC3	3.913	CCR1	2.356
FGF10	3.868	MYCBPAP	2.313
CAMK2A	3.606	TRIM9	2.282
ASIP	3.603	FKBP1B	2.225
RAB3A	3.389	LIN7A	2.212
NPFF	3.274	NRXN3	2.167
GUCA1B	3.201	MPZ	2.154
CCL26	3.073	KCNK3	2.150
ILDR2	3.062	PCLO	2.100
SLC17A7	3.054	VAX2	2.069
NLGN1	2.833	C12orf76	2.065
TRABD2B	2.817	POMC	2.044
WNT2	2.747	RIMS3	2.017

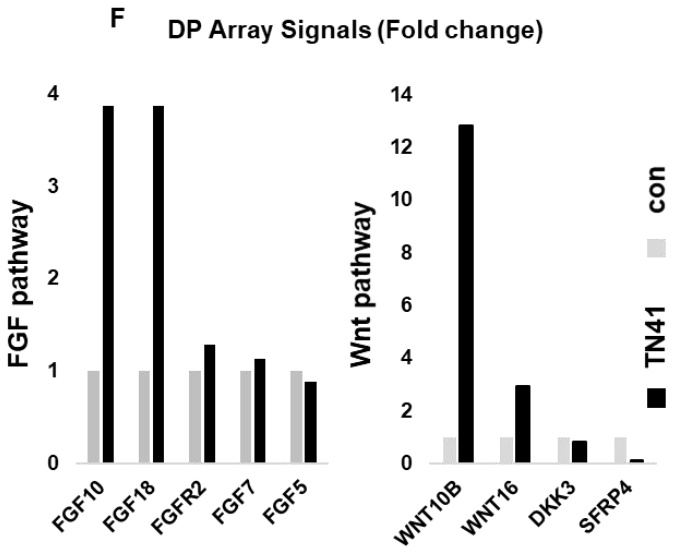

A. Human hair follicle were cultured 6 days with TN41 (20nM). Hair length was

measured by microscopy (N>20). Image of human hair follicles.

***: P<0.001 (Student's t test).

B. IF image of human hair follicle for the Ki67.

C. 3D-spheroid of DPC were injected into epidermis of nude mice. Image obtained after 2 weeks.

D. Gene Ontology comparisons reveal several gene categories enriched progressively as the activation of DP. Note the extracellular signaling molecules were among the most enriched of the specialized categories (Blue box). Fold change >2, P<0.05.

E. List of DPC genes belonging to the extracellular signaling category and that are up-regulated (>2x) with signal values at TN41-treated versus non-treated gene set.

F. Microarray DPC signal values of FGF and WNT pathway members, which displayed particularly prominent temporal differences.

Table 1. The top 50 up-regulated genes by TN41.

	Gene Symbol	Fold change	Normalized data (log_2)		Gene Description
			0h	12h	
	Up regulated gene				
1	PPP4R1-AS1	14.626	0.090	3.960	PPP4R1 antisense RNA 1
2	HYAL1	14.417	0.107	3.957	hyaluronoglucosaminidase 1
3	RNF43	13.650	1.139	4.910	ring finger protein 43
4	ALS2CL	13.508	1.723	5.479	ALS2 C-terminal like
5	RUNX1-IT1	13.285	0.127	3.859	RUNX1 intronic transcript 1
6	UBAP1L	12.986	0.071	3.770	ubiquitin associated protein 1 like
7	WNT10B	12.832	0.085	3.767	Wnt family member 10B
8	AGER	12.832	0.085	3.767	advanced glycosylation end product-specific receptor
9	AGMO	12.735	0.094	3.765	alkylglycerol monooxygenase
10	SGOL1-AS1	12.643	0.103	3.763	
11	SP7	12.102	0.066	3.664	Sp7 transcription factor
12	CCDC151	11.731	0.103	3.655	coiled-coil domain containing 151
13	TTC39C-AS1	11.610	0.115	3.653	TTC39C antisense RNA 1
14	MYH3	11.212	0.061	3.548	myosin, heavy chain 3, skeletal muscle, embryonic
15	MAB21L3	11.163	1.121	4.602	mab-21 like 3
16	C3orf35	11.117	0.071	3.546	chromosome 3 open reading frame 35
17	RBM24	11.027	0.081	3.544	RNA binding motif protein 24
18	SGOL1	10.871	1.152	4.594	
19	PLIN1	10.317	0.056	3.423	perilipin 1
20	ATE1-AS1	10.226	0.066	3.421	ATE1 antisense RNA 1
21	C10orf107	10.141	0.076	3.418	chromosome 10 open reading frame 107
22	MAGI2-AS2	10.060	0.085	3.416	MAGI2 antisense RNA 2
23	CEACAM19	9.982	0.094	3.414	carcinoembryonic antigen related cell adhesion molecule 19
24	MAMDC4	9.872	1.114	4.418	MAM domain containing 4
25	STK33	9.480	1.107	4.352	serine/threonine kinase 33
26	ADAM32	9.415	0.051	3.286	ADAM metallopeptidase domain 32
27	GLIS3-AS1	9.415	0.051	3.286	GLIS3 antisense RNA 1
28	KIF12	9.415	0.051	3.286	kinesin family member 12
29	LOC643542	9.330	0.061	3.283	uncharacterized LOC643542
30	SNORA74B	9.289	0.066	3.282	small nucleolar RNA, H/ACA box 74B
31	CLDN2	9.249	0.071	3.281	claudin 2
32	FBXO41	9.136	0.085	3.277	F-box protein 41
33	LOC100507634	9.101	0.090	3.276	uncharacterized LOC100507634
34	LOC100507334	9.032	0.099	3.274	two pore channel 3 pseudogene
35	LINC01497	8.507	0.046	3.135	long intergenic non-protein coding RNA 1497
36	COL17A1	8.467	0.051	3.133	collagen type XVII alpha 1
37	OTOGL	8.467	0.051	3.133	otogelin like
38	LOC100505716	8.467	0.051	3.133	uncharacterized LOC100505716
39	UNC13D	8.467	0.051	3.133	unc-13 homolog D
40	DYNC1I1	8.427	0.056	3.131	dynein cytoplasmic 1 intermediate chain 1
41	TM4SF19-TCTEX1D2	8.352	0.066	3.129	TM4SF19-TCTEX1D2 readthrough (NMD candidate)
42	ITGB1BP2	8.352	0.066	3.129	integrin subunit beta 1 binding protein 2
43	JPH3	8.316	0.071	3.127	junctophilin 3
44	ADH6	8.119	0.099	3.120	alcohol dehydrogenase 6 (class V)
45	CCDC148	7.968	1.712	4.707	coiled-coil domain containing 148
46	LOC101928324	7.678	1.104	4.045	uncharacterized LOC101928324
47	LOC101929577	7.660	1.107	4.044	uncharacterized LOC101929577
48	B4GALT6	7.563	1.121	4.040	beta-1,4-galactosyltransferase 6
49	SLC25A27	7.494	3.434	6.340	solute carrier family 25 member 27
50	LOC101927811	7.240	1.102	3.958	uncharacterized LOC101927811

Table 2. The top 50 down-regulated genes by TN41.

	Gene Symbol	Fold change	Normalized data (log_2)		Gene Description
			0h	12h	
	Down regulated gene				
1	RSAD2	0.061	4.047	0.000	radical S-adenosyl methionine domain containing 2
2	CEACAM5	0.064	3.960	0.000	carcinoembryonic antigen related cell adhesion molecule 5
3	ANKRD20A9P	0.070	4.707	0.863	ankyrin repeat domain 20 family member A9, pseudogene
4	PARK2	0.074	3.758	0.000	parkin RBR E3 ubiquitin protein ligase
5	RIMKLA	0.080	3.638	0.000	ribosomal modification protein rimK-like family member A
6	AMIGO1	0.080	3.637	0.000	adhesion molecule with Ig-like domain 1
7	TEDDM1	0.081	3.634	0.000	transmembrane epididymal protein 1
8	LINC01122	0.081	3.634	0.000	long intergenic non-protein coding RNA 1122
9	LOC101928069	0.081	3.630	0.000	uncharacterized LOC101928069
10	JPH1	0.087	3.515	0.000	junctophilin 1
11	FAM21EP	0.088	3.511	0.000	family with sequence similarity 21 member E, pseudogene
12	SNORD15A	0.088	3.504	0.000	small nucleolar RNA, C/D box 15A
13	ALDH1A1	0.088	3.504	0.000	aldehyde dehydrogenase 1 family member A1
14	NME2	0.096	3.374	0.000	NME/NM23 nucleoside diphosphate kinase 2
15	CFI	0.096	3.374	0.000	complement factor I
16	SGCG	0.097	3.371	0.000	sarcoglycan gamma
17	DUSP26	0.097	3.366	0.000	dual specificity phosphatase 26 (putative)
18	DNER	0.106	3.232	0.000	delta/notch like EGF repeat containing
19	ZNF485	0.107	3.230	0.000	zinc finger protein 485
20	CALHM1	0.107	3.219	0.000	calcium homeostasis modulator 1
21	AIM2	0.108	3.217	0.000	absent in melanoma 2
22	LINC01363	0.108	3.215	0.000	long intergenic non-protein coding RNA 1363
23	HGFAC	0.108	3.213	0.000	HGF activator
24	GRP	0.108	3.213	0.000	gastrin releasing peptide
25	C4orf19	0.113	4.056	0.906	chromosome 4 open reading frame 19
26	SH2D5	0.113	4.055	0.908	SH2 domain containing 5
27	LINC01530	0.117	3.973	0.882	long intergenic non-protein coding RNA 1530
28	LOC101927964	0.120	3.063	0.000	uncharacterized LOC101927964
29	SGK223	0.120	3.056	0.000	homolog of rat pragma of Rnd2
30	CHRDL1	0.120	3.054	0.000	chordin-like 1
31	ARHGEF38	0.121	3.053	0.000	Rho guanine nucleotide exchange factor 38
32	SHE	0.121	3.049	0.000	Src homology 2 domain containing E
33	LOC101927829	0.121	3.047	0.000	uncharacterized LOC101927829
34	LINC00992	0.121	3.047	0.000	long intergenic non-protein coding RNA 992
35	BTBD18	0.121	3.045	0.000	BTB domain containing 18
36	GLB1L3	0.121	3.045	0.000	galactosidase beta 1 like 3
37	LOC100506869	0.121	3.045	0.000	uncharacterized LOC100506869
38	SNORD36C	0.121	3.045	0.000	small nucleolar RNA, C/D box 36C
39	CA8	0.121	3.045	0.000	carbonic anhydrase 8
40	LRRTM4	0.121	3.043	0.000	leucine rich repeat transmembrane neuronal 4
41	NTS	0.121	3.043	0.000	neurotensin
42	SFRP4	0.121	3.043	0.000	secreted frizzled related protein 4
43	GVINP1	0.124	4.513	1.497	GTPase, very large interferon inducible pseudogene 1
44	TM4SF1	0.131	3.856	0.927	transmembrane 4 L six family member 1
45	TSPAN7	0.136	4.378	1.495	tetraspanin 7
46	SNORD54	0.138	3.760	0.906	small nucleolar RNA, C/D box 54
47	CITED4	0.139	5.925	3.076	Cbp/p300 interacting transactivator with Glu/Asp rich carboxy-terminal domain 4
48	SRCIN1	0.141	3.751	0.925	SRC kinase signaling inhibitor 1
49	CRMP1	0.141	3.750	0.927	collapsin response mediator protein 1
50	RBM46	0.141	3.750	0.927	RNA binding motif protein 46

Discussion

AIMP1 was identified as one of three auxiliary factors of a mammalian aminoacyl tRNA synthetase [10]. AIMP1 binds to and facilitates the catalytic reaction of arginyl-tRNA synthetase [66]. AIMP1 is involved in diverse physiological processes, particularly skin homeostasis. AIMP1 induces the proliferation of fibroblasts and collagen synthesis to improve wound healing [12]. AIMP1 also shows biphasic activity to regulate angiogenesis via the migration of endothelial cells [17]. It also resides in the endoplasmic reticulum, where it retains heat-shock protein gp96 to prevent its aberrant extracellular exposure, which may trigger autoimmune phenotypes [67]. Moreover, AIMP1 enhances the proliferation of bone marrow-derived MSCs via FGFR2-mediated accumulation of beta-catenin [20]. Based on this information, we first identified the function of AIMP1 in the HF environment.

Recent findings have revealed the complexity of cellular and molecular regulators within the skin stem cell niche during development, homeostasis, injury, and aging. However, although many putative niche factors have been identified, the crosstalk between HFSCs and DPCs remained unclear. Some factors regulate HFSCs from DPCs, but SHH was the only well-defined molecule modulating the opposite process. DPCs play an essential role in maintaining the HF niche; however, SHH is not sufficient to explain this. In this study, we identified important factors that modulate

DPCs via specific receptors. Second, although several cell types, including blood vessels and immune cells, make stereotypic and spatially distinct contacts with epithelial cells, the specific signals governing these connections remain unclear [68–71]. The homeostatic function of AIMP1 may provide insight into this process.

Overall, our results support that AIMP1 participates in regulating HF and hair cycling. Indeed, AIMP1−K14 cre mice show hair dysfunctions, while K14−AIMP1 cTg mice show excessive tissue regeneration. Moreover, neogenesis of HFs from nude mice following AIMP1 treatment of human DPCs suggest that AIMP1 can be a novel target to overcome hair loss.

References

1. Cotsarelis, G., T.T. Sun, and R.M. Lavker, *Label-retaining cells reside in the bulge area of pilosebaceous unit: implications for follicular stem cells, hair cycle, and skin carcinogenesis.* Cell, 1990. **61**(7): p. 1329-37.
2. Fuchs, E., *The tortoise and the hair: slow-cycling cells in the stem cell race.* Cell, 2009. **137**(5): p. 811-9.
3. Deschene, E.R., et al., *beta-Catenin activation regulates tissue growth non-cell autonomously in the hair stem cell niche.* Science, 2014. **343**(6177): p. 1353-6.
4. Giangreco, A., et al., *Epidermal stem cells are retained in vivo throughout skin aging.* Aging Cell, 2008. **7**(2): p. 250-9.
5. Doles, J., et al., *Age-associated inflammation inhibits epidermal stem cell function.* Genes Dev, 2012. **26**(19): p. 2144-53.
6. Keyes, B.E., et al., *Nfatc1 orchestrates aging in hair follicle stem cells.* Proc Natl Acad Sci U S A, 2013. **110**(51): p. E4950-9.
7. Chen, C.C., et al., *Regenerative hair waves in aging mice and extra-follicular modulators follistatin, dkk1, and sfrp4.* J Invest Dermatol, 2014. **134**(8): p. 2086-2096.
8. Bhattacharyya, T.K. and J.R. Thomas, *Histomorphologic changes in aging skin: observations in the CBA mouse model.* Arch Facial Plast Surg, 2004. **6**(1): p. 21-5.
9. Smith, L., *Histopathologic characteristics and ultrastructure of aging skin.* Cutis, 1989. **43**(5): p. 414-24.
10. Quevillon, S., et al., *The p43 component of the mammalian multi-synthetase complex is likely to be the precursor of the endothelial monocyte-activating polypeptide II cytokine.* J Biol Chem, 1997. **272**(51): p. 32573-9.
11. Matschurat, S., et al., *Regulation of EMAP II by hypoxia.* Am J Pathol, 2003. **162**(1): p. 93-103.
12. Park, S.G., et al., *The novel cytokine p43 stimulates dermal fibroblast proliferation and wound repair.* Am J Pathol, 2005. **166**(2): p. 387-98.
13. Kim, E., et al., *AIMP1/p43 protein induces the maturation of bone marrow-derived dendritic cells with T helper type 1-polarizing ability.* J Immunol, 2008. **180**(5): p. 2894-902.
14. Kim, E., et al., *The novel cytokine p43 induces IL-12 production in macrophages via NF-kappaB activation, leading to enhanced IFN-gamma production in CD4+ T cells.* J Immunol, 2006. **176**(1): p. 256-64.
15. Ko, Y.G., et al., *A cofactor of tRNA synthetase, p43, is secreted to up-regulate proinflammatory genes.* J Biol Chem, 2001. **276**(25): p. 23028-33.
16. Park, H., et al., *Monocyte cell adhesion induced by a human aminoacyl-tRNA synthetase-*

associated factor, p43: identification of the related adhesion molecules and signal pathways. J Leukoc Biol, 2002. **71**(2): p. 223-30.

17. Park, S.G., et al., *Dose-dependent biphasic activity of tRNA synthetase-associating factor, p43, in angiogenesis.* J Biol Chem, 2002. **277**(47): p. 45243-8.
18. Park, S.G., et al., *Hormonal activity of AIMP1/p43 for glucose homeostasis.* Proc Natl Acad Sci U S A, 2006. **103**(40): p. 14913-8.
19. Han, J.M., et al., *Structural separation of different extracellular activities in aminoacyl-tRNA synthetase-interacting multi-functional protein, p43/AIMP1.* Biochem Biophys Res Commun, 2006. **342**(1): p. 113-8.
20. Kim, S.Y., et al., *ARS-interacting multi-functional protein 1 induces proliferation of human bone marrow-derived mesenchymal stem cells by accumulation of beta-catenin via fibroblast growth factor receptor 2-mediated activation of Akt.* Stem Cells Dev, 2013. **22**(19): p. 2630-40.
21. Petiot, A., et al., *A crucial role for Fgfr2-IIIb signalling in epidermal development and hair follicle patterning.* Development, 2003. **130**(22): p. 5493-501.
22. Fujimoto, A., et al., *FGFR2 is associated with hair thickness in Asian populations.* J Hum Genet, 2009. **54**(8): p. 461-5.
23. Yang, J., et al., *Fibroblast growth factor receptors 1 and 2 in keratinocytes control the epidermal barrier and cutaneous homeostasis.* J Cell Biol, 2010. **188**(6): p. 935-52.
24. Katoh, M., *FGFR2 abnormalities underlie a spectrum of bone, skin, and cancer pathologies.* J Invest Dermatol, 2009. **129**(8): p. 1861-7.
25. Jeon, Y., et al., *TopBP1 deficiency causes an early embryonic lethality and induces cellular senescence in primary cells.* J Biol Chem, 2011. **286**(7): p. 5414-22.
26. Kruger, N.J., *The Bradford method for protein quantitation.* Methods Mol Biol, 1994. **32**: p. 9-15.
27. Zheng, Y., et al., *Organogenesis from dissociated cells: generation of mature cycling hair follicles from skin-derived cells.* J Invest Dermatol, 2005. **124**(5): p. 867-76.
28. Philpott, M.P., et al., *Human hair growth in vitro: a model for the study of hair follicle biology.* J Dermatol Sci, 1994. **7 Suppl**: p. S55-72.
29. Magerl, M., et al., *Simple and rapid method to isolate and culture follicular papillae from human scalp hair follicles.* Exp Dermatol, 2002. **11**(4): p. 381-5.
30. Porter, R.M., *Mouse models for human hair loss disorders.* J Anat, 2003. **202**(1): p. 125-31.
31. Matsumura, H., et al., *Hair follicle aging is driven by transepidermal elimination of stem cells via COL17A1 proteolysis.* Science, 2016. **351**(6273): p. aad4395.
32. Lay, K., T. Kume, and E. Fuchs, *FOXC1 maintains the hair follicle stem cell niche and governs stem cell quiescence to preserve long-term tissue-regenerating potential.* Proc Natl Acad Sci U S A, 2016. **113**(11): p. E1506-15.

33. Plikus, M.V. and C.M. Chuong, *Complex hair cycle domain patterns and regenerative hair waves in living rodents.* J Invest Dermatol, 2008. **128**(5): p. 1071-80.
34. Huelsken, J., et al., *beta-Catenin controls hair follicle morphogenesis and stem cell differentiation in the skin.* Cell, 2001. **105**(4): p. 533-45.
35. Enshell-Seijffers, D., et al., *Beta-catenin activity in the dermal papilla of the hair follicle regulates pigment-type switching.* Proc Natl Acad Sci U S A, 2010. **107**(50): p. 21564-9.
36. Enshell-Seijffers, D., et al., *beta-catenin activity in the dermal papilla regulates morphogenesis and regeneration of hair.* Dev Cell, 2010. **18**(4): p. 633-42.
37. Kishimoto, J., R.E. Burgeson, and B.A. Morgan, *Wnt signaling maintains the hair-inducing activity of the dermal papilla.* Genes Dev, 2000. **14**(10): p. 1181-5.
38. Kwon, H.S., et al., *Identification of CD23 as a functional receptor for the proinflammatory cytokine AIMP1/p43.* J Cell Sci, 2012. **125**(Pt 19): p. 4620-9.
39. Popko, K., et al., *Proinflammatory cytokines Il-6 and TNF-alpha and the development of inflammation in obese subjects.* Eur J Med Res, 2010. **15 Suppl 2**: p. 120-2.
40. Starling, S., *Regulatory T cells: Keep your hair on.* Nat Rev Immunol, 2017. **17**(7): p. 402-403.
41. Ali, N., et al., *Regulatory T Cells in Skin Facilitate Epithelial Stem Cell Differentiation.* Cell, 2017. **169**(6): p. 1119-1129 e11.
42. Magro, C.M., et al., *The role of inflammation and immunity in the pathogenesis of androgenetic alopecia.* J Drugs Dermatol, 2011. **10**(12): p. 1404-11.
43. Messenger, A.G. and J. Rundegren, *Minoxidil: mechanisms of action on hair growth.* Br J Dermatol, 2004. **150**(2): p. 186-94.
44. Meephansan, J., et al., *Efficacy of topical tofacitinib in promoting hair growth in non-scarring alopecia: possible mechanism via VEGF induction.* Arch Dermatol Res, 2017. **309**(9): p. 729-738.
45. Park, S.G., E.C. Choi, and S. Kim, *Aminoacyl-tRNA synthetase-interacting multifunctional proteins (AIMPs): a triad for cellular homeostasis.* IUBMB Life, 2010. **62**(4): p. 296-302.
46. Won, C.H., et al., *Comparative secretome analysis of human follicular dermal papilla cells and fibroblasts using shotgun proteomics.* BMB Rep, 2012. **45**(4): p. 253-8.
47. Schilling, O. and C.M. Overall, *Proteome-derived, database-searchable peptide libraries for identifying protease cleavage sites.* Nat Biotechnol, 2008. **26**(6): p. 685-94.
48. Yang, C.C. and G. Cotsarelis, *Review of hair follicle dermal cells.* J Dermatol Sci, 2010. **57**(1): p. 2-11.
49. Iida, M., S. Ihara, and T. Matsuzaki, *Hair cycle-dependent changes of alkaline phosphatase activity in the mesenchyme and epithelium in mouse vibrissal follicles.* Dev Growth Differ, 2007. **49**(3): p. 185-95.
50. Zhang, P., et al., *A review of adipocyte lineage cells and dermal papilla cells in hair follicle regeneration.* J Tissue Eng, 2014. **5**: p. 2041731414556850.

51. Lee, S.H., et al., *Valproic acid induces hair regeneration in murine model and activates alkaline phosphatase activity in human dermal papilla cells.* PLoS One, 2012. **7**(4): p. e34152.
52. Yamao, M., et al., *Contact between dermal papilla cells and dermal sheath cells enhances the ability of DPCs to induce hair growth.* J Invest Dermatol, 2010. **130**(12): p. 2707-18.
53. Li, Y.H., et al., *Wnt10b promotes growth of hair follicles via a canonical Wnt signalling pathway.* Clin Exp Dermatol, 2011. **36**(5): p. 534-40.
54. Li, Y.H., et al., *Adenovirus-mediated Wnt10b overexpression induces hair follicle regeneration.* J Invest Dermatol, 2013. **133**(1): p. 42-8.
55. Guo, H., et al., *Secreted Frizzled-related protein 4 inhibits the regeneration of hair follicles.* PeerJ, 2019. **6**: p. e6153.
56. Greco, V., et al., *A two-step mechanism for stem cell activation during hair regeneration.* Cell Stem Cell, 2009. **4**(2): p. 155-69.
57. Lei, M.X., C.M. Chuong, and R.B. Widelitz, *Tuning Wnt signals for more or fewer hairs.* J Invest Dermatol, 2013. **133**(1): p. 7-9.
58. Teh, M.T., et al., *Role for WNT16B in human epidermal keratinocyte proliferation and differentiation.* J Cell Sci, 2007. **120**(Pt 2): p. 330-9.
59. Lim, X., et al., *Axin2 marks quiescent hair follicle bulge stem cells that are maintained by autocrine Wnt/beta-catenin signaling.* Proc Natl Acad Sci U S A, 2016. **113**(11): p. E1498-505.
60. Nakamura, R.E. and A.S. Hackam, *Analysis of Dickkopf3 interactions with Wnt signaling receptors.* Growth Factors, 2010. **28**(4): p. 232-42.
61. Guo, L., L. Degenstein, and E. Fuchs, *Keratinocyte growth factor is required for hair development but not for wound healing.* Genes Dev, 1996. **10**(2): p. 165-75.
62. Suzuki, K., et al., *Defective terminal differentiation and hypoplasia of the epidermis in mice lacking the Fgf10 gene.* FEBS Lett, 2000. **481**(1): p. 53-6.
63. Werner, S., et al., *The function of KGF in morphogenesis of epithelium and reepithelialization of wounds.* Science, 1994. **266**(5186): p. 819-22.
64. Kawano, M., et al., *Comprehensive analysis of FGF and FGFR expression in skin: FGF18 is highly expressed in hair follicles and capable of inducing anagen from telogen stage hair follicles.* J Invest Dermatol, 2005. **124**(5): p. 877-85.
65. Ota, Y., et al., *Fibroblast growth factor 5 inhibits hair growth by blocking dermal papilla cell activation.* Biochem Biophys Res Commun, 2002. **290**(1): p. 169-76.
66. Park, S.G., et al., *Precursor of pro-apoptotic cytokine modulates aminoacylation activity of tRNA synthetase.* J Biol Chem, 1999. **274**(24): p. 16673-6.
67. Han, J.M., et al., *Aminoacyl-tRNA synthetase-interacting multifunctional protein 1/p43 controls endoplasmic reticulum retention of heat shock protein gp96: its pathological implications in lupus-like autoimmune diseases.* Am J Pathol, 2007. **170**(6): p. 2042-54.

68. Janich, P., et al., *Human epidermal stem cell function is regulated by circadian oscillations.* Cell Stem Cell, 2013. **13**(6): p. 745-53.
69. Janich, P., et al., *The circadian molecular clock creates epidermal stem cell heterogeneity.* Nature, 2011. **480**(7376): p. 209-14.
70. Goldstein, J., et al., *Calcineurin/Nfatc1 signaling links skin stem cell quiescence to hormonal signaling during pregnancy and lactation.* Genes Dev, 2014. **28**(9): p. 983-94.
71. McGee, H.M., et al., *IL-22 promotes fibroblast-mediated wound repair in the skin.* J Invest Dermatol, 2013. **133**(5): p. 1321-9.